ARMY RESEARCH LABORATORY



Ordered and Highly Scalable Granular Media for Shock Mitigation

by Robert Doney and Surajit Sen

ARL-TR-3612 **September 2005**

Approved for public release; distribution is unlimited.

AUTHENTICATED
U.S. GOVERNMENT
INFORMATION
GPO

NOTICES

Disclaimers

The findings in this report are not to be construed as an official Department of the Army position unless so designated by other authorized documents.

Citation of manufacturer's or trade names does not constitute an official endorsement or approval of the use thereof.

Destroy this report when it is no longer needed. Do not return it to the originator.

Army Research Laboratory
Aberdeen Proving Ground, MD 21005-5066

ARL-TR-3612 **September 2005**

Ordered and Highly Scalable Granular Media for Shock Mitigation

Robert Doney
Weapons and Materials Research Directorate, ARL

Surajit Sen
State University of New York, Buffalo, NY

Approved for public release; distribution is unlimited.

REPORT DOCUMENTATION PAGE	Form Approved OMB No. 0704-0188

Public reporting burden for this collection of information is estimated to average 1 hour per response, including the time for reviewing instructions, searching existing data sources, gathering and maintaining the data needed, and completing and reviewing the collection information. Send comments regarding this burden estimate or any other aspect of this collection of information, including suggestions for reducing the burden, to Department of Defense, Washington Headquarters Services, Directorate for Information Operations and Reports (0704-0188), 1215 Jefferson Davis Highway, Suite 1204, Arlington, VA 22202-4302. Respondents should be aware that notwithstanding any other provision of law, no person shall be subject to any penalty for failing to comply with a collection of information if it does not display a currently valid OMB control number.
PLEASE DO NOT RETURN YOUR FORM TO THE ABOVE ADDRESS.

1. REPORT DATE *(DD-MM-YYYY)*	2. REPORT TYPE	3. DATES COVERED (From - To)
September 2005	Final	June 2004–April 2005

4. TITLE AND SUBTITLE	5a. CONTRACT NUMBER
Ordered and Highly Scalable Granular Media for Shock Mitigation	5b. GRANT NUMBER
	5c. PROGRAM ELEMENT NUMBER

6. AUTHOR(S)	5d. PROJECT NUMBER
Robert Doney and Surajit Sen*	AH80
	5e. TASK NUMBER
	5f. WORK UNIT NUMBER

7. PERFORMING ORGANIZATION NAME(S) AND ADDRESS(ES)	8. PERFORMING ORGANIZATION REPORT NUMBER
U.S. Army Research Laboratory ATTN: AMSRD-ARL-WM-TA Aberdeen Proving Ground, MD 21005-5066	ARL-TR-3612

9. SPONSORING/MONITORING AGENCY NAME(S) AND ADDRESS(ES)	10. SPONSOR/MONITOR'S ACRONYM(S)
	11. SPONSOR/MONITOR'S REPORT NUMBER(S)

12. DISTRIBUTION/AVAILABILITY STATEMENT

Approved for public release; distribution is unlimited.

13. SUPPLEMENTARY NOTES

*State University of New York, Buffalo, NY

14. ABSTRACT

We provide an update to our current efforts in studying shock mitigation using one-dimensional arrays of adjacent metal spheres that may progressively shrink in size. These tapered chains are characterized by the number of spheres, N, the amount of tapering, q, and restitutive losses, ω. Spheres are assumed to interact via the nonlinear Hertz potential, $V \alpha \delta^{5/2}$, where δ is the amount of overlap of adjacent grains and the constant of proportionality varies with the material. To gauge the ability of such chains to absorb transient pulses, we look at the normalized kinetic energy, KE_N, as a function of N, q, ω. A hard-sphere approximation and numerical analysis is therefore performed for $3 \leq N \leq 20$ and $0 \leq q, \omega \leq 0.1$ for two tapered chain architectures. Intended experimental studies are outlined as those that have already been performed and focus on solitary wave propagation in monodisperse ($q = 0$) chains. Results are quite encouraging and independent of system size; consequently, we propose a tapered chain armor panel design consisting of many tapered chains working in tandem. The specific and gravimmetric absorbed energies are calculated for an example prototype. Intended work and further discussion are provided in the conclusion.

15. SUBJECT TERMS

shock, mitigation, granular media, ballistic shock, Hertz, tapered chain, solitary wave

16. SECURITY CLASSIFICATION OF:			17. LIMITATION OF ABSTRACT	18. NUMBER OF PAGES	19a. NAME OF RESPONSIBLE PERSON
a. REPORT	b. ABSTRACT	c. THIS PAGE			Robert Doney
UNCLASSIFIED	UNCLASSIFIED	UNCLASSIFIED	UL	68	19b. TELEPHONE NUMBER (*Include area code*) 410-278-7309

Standard Form 298 (Rev. 8/98)
Prescribed by ANSI Std. Z39.18

Contents

List of Figures v

List of Tables vi

1. Introduction 1

2. Granular Media and TCs 1

3. Hard-Sphere Approximation 3

3.1 The Simple Tapered Chain 3

3.1.1 Lossless STC Hard-Sphere Approximation 3

3.1.2 Lossy STC Hard-Sphere Approximation 4

3.1.3 KE Parameter Space for STC Hard-Spheres 5

3.2 The Decorated Tapered Chain 5

4. Numerical Solution to the Equations of Motion 11

4.1 STC 14

4.1.1 STC KE and Force Parameter Spaces: $\boldsymbol{KE}\left(\boldsymbol{N},\boldsymbol{q},\boldsymbol{\omega}\right),\boldsymbol{F}\left(\boldsymbol{N},\boldsymbol{q},\boldsymbol{\omega}\right)$ 16

4.1.2 STC Mathematical Model 19

4.2 DTC 20

5. Experimental Efforts 22

5.1 STC 22

5.2 DTC 23

6. Precompressed Chains 27

7. TC Armor Panels 28

8. Concluding Remarks 31

9. References 32

Appendix A. Simple Tapered Chain Code **35**

Appendix B. Decorated Tapered Chain Modifications **45**

Appendix C. Practical Extration and Report Language (PERL) Script for Parametric Studies **49**

Appendix D. MATLAB Code for Generating Numerical Kinetic Energy Surfaces **53**

Appendix E. Normalization **57**

Distribution List **58**

List of Figures

Figure 1. The simple tapered chain: $N = 10$, $q = 8\%$, $L = 70.7$ mm, and $r_i = 5$ mm. 2

Figure 2. $KE\ (N,q,E_L)$ parameter space for the STC hard-sphere approximation. N varies from 3 to 25 and q from 0% to 20%. 6

Figure 3. $KE(N,q)$ parameter space for the STC hard-sphere approximation where the initial velocity is supplied to the smaller end of the chain. 7

Figure 4. The decorated tapered chain: $N = 13$, $q = 8\%$, $f = 0.7$, $L = 80.7$ mm, and $r_i = 5$ mm. 7

Figure 5. KE as a function of N,q and f for DTC hard-spheres. Note that the colorscale is calibrated for each subplot. 12

Figure 6. KE as a function of time for the smallest particle in a chain with $N = 20,\ \omega = 0.05,$ and $q = [0 : 0.02 : 0.1]$. Each plot is evaluated for a different tapering with initial KE as 0.0838 J. 15

Figure 7. Numerical solution of $KE(N,q)$ parameter space for constant ω. Note that it would be very difficult and costly to produce a similar plot empirically. Each node on the surface represents a different TC and experiment. 17

Figure 8. Numerical solution of $F(N,q)$ parameter space for constant ω. 18

Figure 9. Difference plot of the lossless KE parameter spaces for the hard-sphere approximation (figure 2a) and numerical solution (7a). Note that the azimuthal view has been rotated 180° for clarity. 19

Figure 10. The simulated and modeled STC. 21

Figure 11. DTC numerical solution of $KE(N,q,f)$ and sample DTCs for various f (inset). The scale is the same as that in figure 7. 22

Figure 12. STC experimental setup by Job et al. (*12*). 23

Figure 13. STC experimental setup. The left half of the figure represents a monodisperse chain while the right a TC. Lower plots denote later time. 24

Figure 14. Preliminary DTC housing chamber. 25

Figure 15. DTC constituents. 26

Figure 16. DTC interstitial grains. 27

Figure 17. KE as a function of tapering and restitution for constant $N = 20$ and $\Delta = 0.03\%$. 28

Figure 18. STC armor plate panel. 29

Figure 19. SAE and VAE as a function of M, the total STC armor panel mass, and u_f, the incident flyer plate velocity. 30

List of Tables

Table 1. Material properties (*28*). 13

1. Introduction

Our recent work (*1*, *2*) in the area of granular physics indicates that certain (ordered with respect to size) arrangements of smooth, metal spheres adjacent to each other in one-dimensional (1-D) chains demonstrate noticeable shock absorption. This has been observed and measured analytically (*1–5*) and through numerical integration of the equations of motion (*1*, *6–8*). Experimental efforts (*9–12*) have focused primarily on solitary wave propagation and demonstrating reduced impact force using tapered chains (TCs) (*4*). The system is scalable, as there does not appear to be any restrictions on particle size. There is, of course, limits imposed by quantum physics and manufacture of the spheres. Up to this point in our efforts, only single chains of varying length have been considered. However, increasingly encouraging results have prompted us to consider the collective disruptive effects of many chains as a defeat mechanism against ballistic shock and other undesirable transient pulses.

The goal of this report is to summarize both published and unpublished results through normalized energy calculations and include an analytical description of a potential armor panel. The contents are organized as follows. A small overview of granular media and the ordered systems of interest are first discussed. This is followed by a hard-sphere approximation and the numerical solution to the equations of motion. In addition, our mathematical model provides some predictive capability for a certain range of systems. Past experimental arrangements and intended investigations are reviewed. In conclusion, we introduce a potential armor panel configuration with an estimate of the specific and volumetric absorbed energy and summarize the salient features of the report.

2. Granular Media and TCs

Granular media (*13–17*)—not to be confused with microscopic grains in a metal—are a curious thing. In general, its members consist of discrete particles that can range in size from micrometers to meters and number in quantity from several to the uncountable. The most well-known constituents of this group are sands and powders and are utilized across many disciplines. In this communication, components of granular media may be referred to as grains, particles, beads, or spheres. These media are particularly intriguing in that among other things it has properties of liquids and solids and calls have been made to add it as a fundamental state of matter (*13*). Within the U.S. Army Research Laboratory, granular media have been investigated for understanding wave propagation and its mathematical similarity to nonlinear rods (*18*).

While granular media have been fundamental in saving lives for decades against ballistics (sandbags), new features are being observed in the growing literature which suggest a more

technological role may be at hand. Particularly appealing and relatively simple to address is the behavior of 1-D systems where smooth elastic spheres intersect at a point in their initial state. Even though we may constrain the basis of variables in this system to just a few parameters, the complexity of its dynamics is formidable. We call these systems tapered chains (TCs).

We define TCs (figure 1) as 1-D granular arrays of elastic spheres that touch at a single point in their initial state and grow to a disk under compression in the plane perpendicular to the figure. The chains can be characterized by the number of grains, N, the successive decrease in size of the grains or tapering, q, and restitutive losses, ω. Restitution (*19–20*) represents the expansion phase in a collision where energy is converted from elastic potential to kinetic and energy losses can be incorporated.

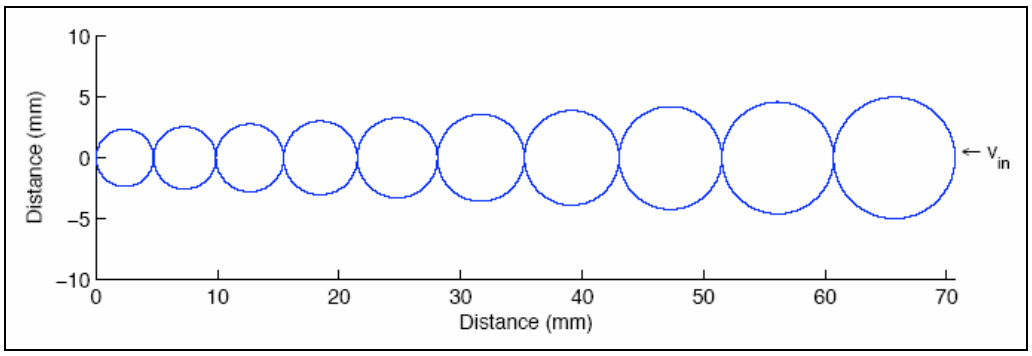


Figure 1. The simple tapered chain: $N = 10$, $q = 8\%$, $L = 70.7$ mm, and $r_i = 5$ mm.

It is intriguing and suggestive that, conceptually, granular media can be envisioned as the inverse of a porous material. In a porous material, there are gaseous (air) voids within a solid matrix. For dry granular media, solid voids (grains) exist within a gaseous matrix (air). Packing, however, limits the analogy; for grains, each entity is in contact with at least one other, whereas voids are not necessarily in contact with one another in porous materials. This is an interesting comparison to draw because the considerable amount of work required to collapse the voids in a porous material makes it a favorable technology against ballistic shock (*21*). Are there then opportunities in granular media for the armor designer to exploit?

The interaction potential between adjacent elastic spheres was first identified by Hertz (*22*) circa 1881. Modern and eloquent derivations were later performed by both Landau and Lifshitz (*23*) and Love (*24*), with a simplified order of magnitude approach by Leroy (*25*). More recently, Nesterenko (*26*) has written extensively on the dynamics of granular chains. If one can show significant reduction in output energy while ensuring that the structure of granular columns can be maintained, it is quite possible to use these TCs against propagating shocks. For now, we assume that one remains within the elastic regime. Future work will begin to relax this restriction.

3. Hard-Sphere Approximation

These approximations differ from the numerically simulated systems in two major ways. The first is that the chain is not bounded by fixed rigid walls. As a result, energy will not continue to be transmitted up and down the chain. The second is that the potential becomes infinite and as a consequence, the energy packet is only 1 grain in width. The system therefore propagates energy as independent collisions. This is congruent to the independent collision model proposed by Wu (*4*). In the numerical results, width of the energy pulse is a function of the tapering—and when all grains are the same size it is about 5 grains wide. By generating an iterative form of the conservation equations, one can arrive at an expression for the normalized kinetic energy (KE), $KE_N = KE_{out}/KE_{in}$. This ratio will be the primary variable determining the absorptive quality of TCs.

3.1 The Simple Tapered Chain

The simple tapered chain (STC) is displayed in figure 1. To generate an initial disturbance, an input velocity, v_i, is applied to the rightmost and largest grain with radius, r_i. It propagates to the left, encountering an initially stationary grain of radius, r_{i+1}. The radius of the $i+1$ particle may be reduced by q% from r_i. This tapering q will be constant along the entire length of the chain. During the transmission of the impulse along the chain, there may be energy losses and we consider two cases described in the following subsections.

3.1.1 Lossless STC Hard-Sphere Approximation

Ignoring any energy loss during a collision, we perform an STC hard-sphere approximation for a TC. Masses and radii are expressed as

$$\begin{aligned} r_{i+1} &= r_i - r_i q = (1-q) r_i = \varepsilon r_i, \\ m_i &= \rho V_i = \frac{4}{3}\pi r_i^3 \rho = \eta r_i^3, \end{aligned} \tag{1}$$

and

$$m_{i+1} = \eta r_{i+1}^3 = \eta \varepsilon^3 r_i^3, \tag{2}$$

where $\varepsilon = 1 - q$. Evaluating the conservation of momentum with a single prime denoting post collision values and the initial condition that the $i+1$ particle is stationary before a collision ($v_{i+1} = 0$), all η cancel and we obtain

$$\begin{aligned} m_i v_i + m_{i+1} v_{i+1} &= m_i v_i' + m_{i+1} v_{i+1}' \\ r_i^3 v_i &= r_i^3 v_i' + \varepsilon^3 r_i^3 v_{i+1}', \\ v_i &= v_i' + \varepsilon^3 v_{i+1}' \end{aligned} \tag{3}$$

where equations 1 and 2 have been used. Following the same procedure for the conservation of energy while ignoring the factor of one-half yields

$$v_i^2 = v_i'^2 + \varepsilon^3 v_{i+1}'^2. \tag{4}$$

Letting $A = \varepsilon^3 v_{i+1}'$, we can rewrite equation 3 in terms of v_i' and substitute the resulting expression into equation 4,

$$\begin{aligned} v_i^2 &= \left(v_i - A\right)^2 + A v_{i+1}' \\ &= v_i^2 - 2Av_i + A^2 + Av_{i+1}', \\ 2v_i &= A + v_{i+1}' \\ \frac{v_{i+1}'}{v_i} &= \frac{2}{1+\varepsilon^3}. \end{aligned} \tag{5}$$

Note that for one collision,

$$\begin{aligned} \frac{KE_{out}}{KE_{in}} = \frac{KE_{i+1}'}{KE_i} = \frac{m_{i+1}}{m_i}\left(\frac{v_{i+1}'}{v_i}\right)^2 = \varepsilon^3\left(\frac{v_{i+1}'}{v_i}\right)^2 \\ \frac{KE_{i+1}'}{KE_i} = \frac{4\varepsilon^3}{\left(1+\varepsilon^3\right)^2}. \end{aligned} \tag{6}$$

For N particles there will be N-1 collisions, each of which has the ratio in equation 6. Therefore, the normalized KE, KE_N, for the lossless STC hard-sphere approximation is given as

$$KE_N = \left\{\frac{4\left(1-q\right)^3}{\left[1+\left(1-q\right)^3\right]^2}\right\}^{N-1}. \tag{7}$$

3.1.2 Lossy STC Hard-Sphere Approximation

The same approximation can be performed with some amount of energy loss, $\tilde{E}_L$, included such that the system is still conservative and may represent a better approximation. Consequently, the momentum equation 3 is unchanged, but equation 4 becomes

$$v_i^2 = v_i'^2 + \varepsilon^3 v_{i+1}'^2 + \tilde{E}_L. \tag{8}$$

One then obtains a more complicated expression replacing equation 5:

$$\frac{v_{i+1}'}{v_i} = \frac{2 - \dfrac{\tilde{E}_L}{\varepsilon^3 v_i v_{i+1}'}}{1+\varepsilon^3}. \tag{9}$$

We can make the substitution, $\tilde{E}_L \propto v_i v_{i+1}'$ or $\tilde{E}_L = E_L v_i v_{i+1}'$, where E_L is the constant of proportionality. This adjustment yields

$$\frac{v'_{i+1}}{v_i} = \frac{2\varepsilon^3 - E_L}{\varepsilon^3\left(1+\varepsilon^3\right)} \ .$$

The corresponding result for the normalized KE for N particles is

$$KE_N = \left\{ \frac{\left[2(1-q)^3 - E_L\right]^2}{(1-q)^3\left[1+(1-q)^3\right]^2} \right\}^{N-1} \ . \tag{10}$$

In the limit $E_L = 0$, equation 10 reduces to the lossless case, equation 7, as one would expect. Note that results are independent of initial velocity and size of the grains.

3.1.3 KE Parameter Space for STC Hard-Spheres

Figure 2 highlights the behavior of equation 10 for $0 \le q \le 0.1$, $3 \le N \le 20$ and selected E_L. The tapering q resembles a sigmoid or half-gaussian and is stretched to infinity for small N. In the limits that $q = 0$ or $N = 1$ (not shown), KE is unity. For the lossless, monodisperse chain (panel (a), $q = 0$), that energy is completely transferred regardless of the number of spheres.

Interestingly, if the initial velocity is supplied to the smaller end of the TC, one also observes shock absorption similar to the system in figure 1, albeit with less efficiency. This is accomplished by adjusting the definition of tapering. In this case, subsequent particles are growing in size, i.e., $r_{i+1} = (1 + q)r_i$. Equations 7 and 10 are modified accordingly, and the result for a lossless system is illustrated in figure 3. Apparently, both configurations mitigate a propagating pulse.

3.2 The Decorated Tapered Chain

The second and last TC geometry that we consider is the decorated tapered chain (DTC) (figure 4). This can be assembled from the STC by introducing a single-sized interstitial grain of radius r_{even} between every member of an STC. We constrain the system to an odd number of particles such that the inserted grains are not at the boundary. Additionally, we presume that these interstitial grains will be equal to or smaller than the smallest member (r_N) of the tapered part of the chain; therefore, $r_{even} = fr_N$, where $0 < f \le 1.0$—although the flexibility is already built in for f to be any size.

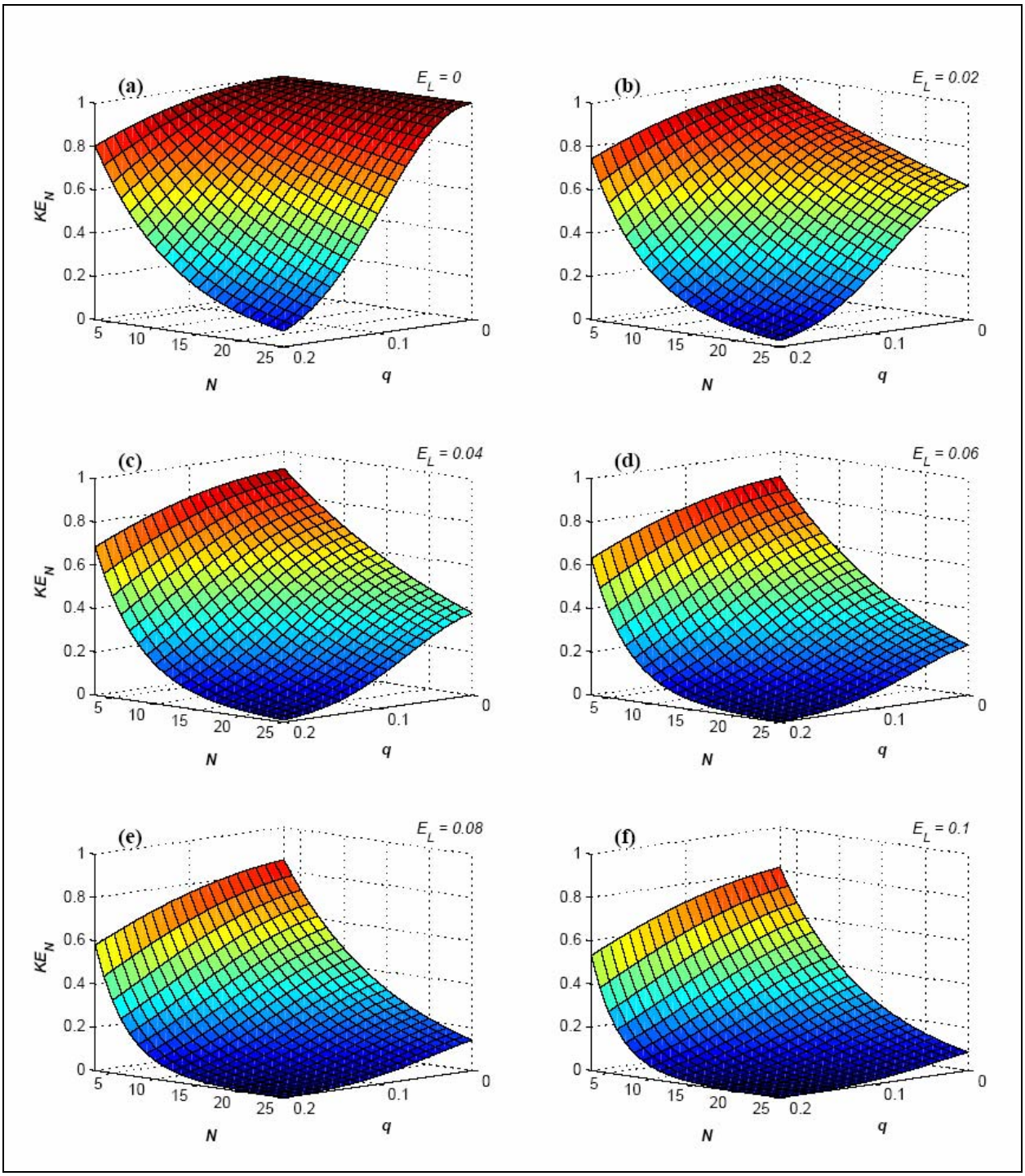


Figure 2. KE (N,q,E_L) parameter space for the STC hard-sphere approximation. N varies from 3 to 25 and q from 0% to 20%.

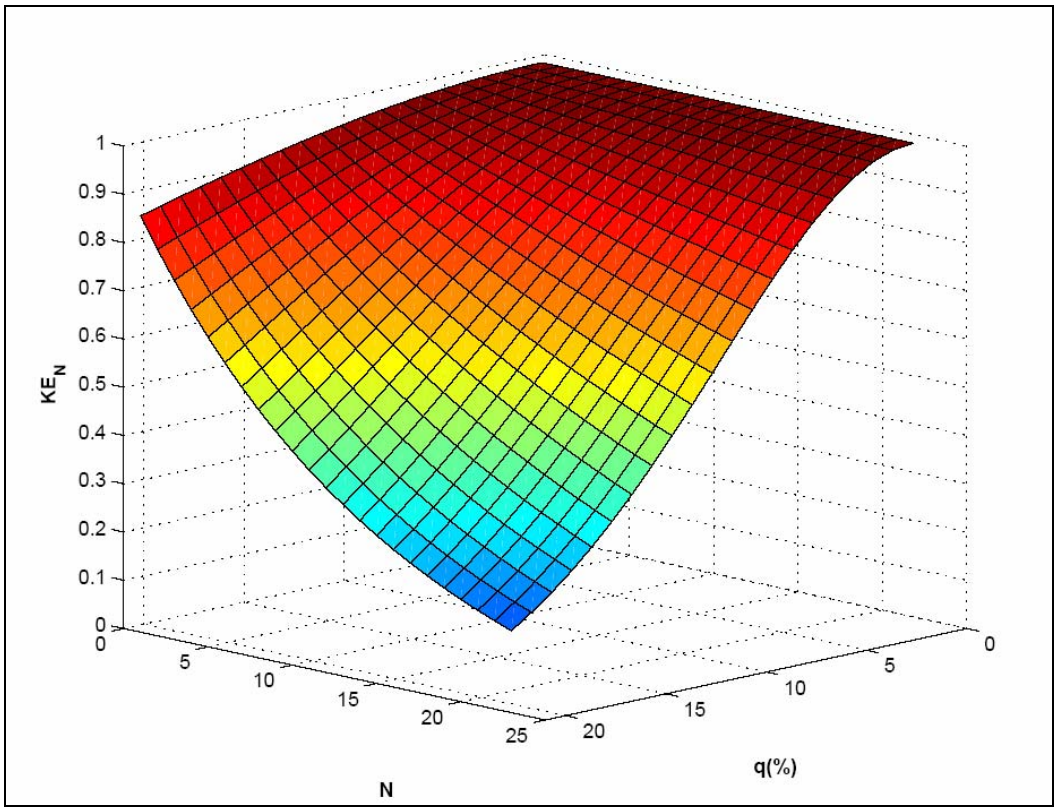


Figure 3. $KE(N,q)$ parameter space for the STC hard-sphere approximation where the initial velocity is supplied to the smaller end of the chain.

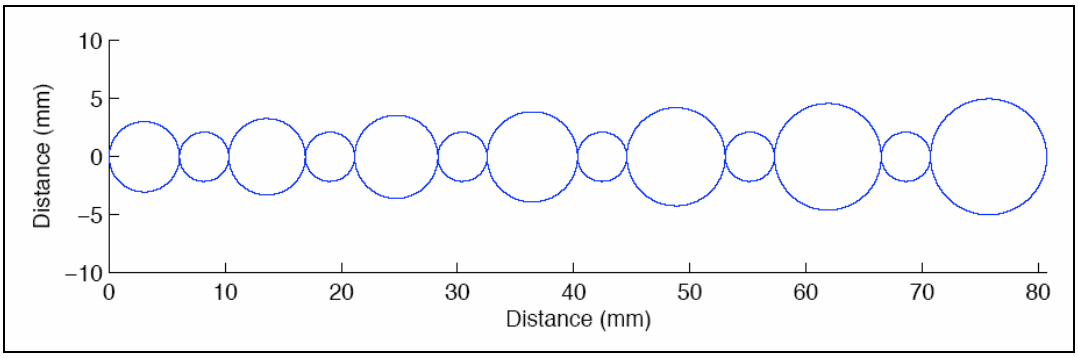


Figure 4. The decorated tapered chain: $N = 13$, $q = 8\%$, $f = 0.7$, $L = 80.7$ mm, and $r_i = 5$ mm.

It is immediately clear that size mismatch between neighboring grains is a function of position along the DTC. This is in stark contrast to the STC, where successive grains are always smaller (or larger) by the same amount. It is possible then to have DTC chains that appear to resemble monodisperse chains for only a portion of the chain.

Again, our primary interest is in deriving an expression for the normalized KE,

$$\frac{KE_{out}}{KE_{in}} = \frac{KE_N}{KE_1} = \frac{m_N}{m_1}\left(\frac{v'_N}{v_1}\right)^2 = \frac{m_N}{m_1}\left[\left(\frac{v'_N}{v'_{N-1}}\right)\cdots\left(\frac{v'_{i+2}}{v'_{i+1}}\right)\left(\frac{v'_{i+1}}{v'_i}\right)\cdots\left(\frac{v'_2}{v_1}\right)\right]^2 , \tag{11}$$

which can again be obtained by the conservation of momentum and energy where collisions are treated as independent. Since these are not trivial iterative solutions as in the STC hard-sphere approximation, we must solve for successive collisions and determine the overall pattern. We will eventually look for forms of v'_{i+1}/v_i and then generalize for N particles or $N-1$ collisions. First, the relationship among masses and radii must be evaluated. Given N(odd) particles in a DTC, every other grain will reduce in size by q% such that $r_{i+2} = \varepsilon r_i$, where $\varepsilon = (1-q)$. Assembling the radii, we have

$$r_i \tag{12}$$

$$r_{i+1} = f\, r_N \tag{13}$$

$$r_{i+2} = r_i - q r_i = (1-q) r_i = \varepsilon r_i \tag{14}$$

$$r_{i+3} = f\, r_N \tag{15}$$

$$r_{i+4} = r_{i+2} - q r_{i+2} = (1-q) r_{i+2} = \varepsilon^2 r_i \tag{16}$$

$$r_{i+5} = f\, r_N \tag{17}$$

$$r_{i+6} = r_{i+4} - q r_{i+4} = (1-q) r_{i+4} = \varepsilon^3 r_i \tag{18}$$

$$\vdots$$

$$r_{N-1} = f\, r_N \tag{19}$$

$$r_N = r_{N-2} - q r_{N-2} = (1-q) r_{N-2} = \varepsilon^{(N-1)/2} r_i \tag{20}$$

Equations 12–14 imply $N = 3$, equations 12–16 imply $N = 5$, etc. The major equations for radii are therefore

$$\begin{aligned} r_N &= \varepsilon^{(N-1)/2} r_i \\ r_{(i+1),(i+3),\cdots,(N-1)} &= f\,\varepsilon^{(N-1)/2} r_i \end{aligned} . \tag{21}$$

Recall for masses that $m_i = \rho V_i = \frac{4}{3}\pi r_i^3 \rho = \eta r_i^3$. Note that since η is just a constant and will cancel once the conservation equations are put into use, we will ignore it from now on. This expression for m_i combined with equations for r_i provide the relations

$$\begin{aligned} m_i &\propto \varepsilon^0 r_i^3 \\ m_{i+1} &\propto r_{i+1}^3 = A r_i^3 \\ m_{i+2} &\propto \varepsilon^3 r_i^3 \\ m_{i+3} &\propto r_{i+3}^3 = A r_i^3 \\ m_{i+4} &\propto \varepsilon^6 r_i^3 \\ &\vdots \\ m_{N-1} &\propto r_{N-1}^3 = A r_i^3 \\ m_N &\propto \varepsilon^{3(N-1)/2} r_i^3 \end{aligned} \tag{22}$$

where $A = f^3 \varepsilon^{3(N-1)/2}$. We may now use these to evaluate the conservation equations. Beginning with momentum and assuming that each subsequent particle in the chain begins at rest, we solve for the first five collisions. Primes and double-primes indicate post-collision states. A primed quantity denotes the first post-collision state of a sphere which serves as input to the next collision. To keep track of its velocity after the second collision, it is denoted by a double-prime and will eventually be eliminated. With $\varepsilon = (1-q)$, we obtain

$$m_i v_i = m_i v_i' + m_{i+1} v_{i+1}' \quad \rightarrow \quad v_i = v_i' + A v_{i+1}' \tag{23}$$

$$m_{i+1} v_{i+1}' = m_{i+1} v_{i+1}'' + m_{i+2} v_{i+2}' \quad \rightarrow \quad A v_{i+1}' = A v_{i+1}'' + \varepsilon^3 v_{i+2}' \tag{24}$$

$$m_{i+2} v_{i+2}' = m_{i+2} v_{i+2}'' + m_{i+3} v_{i+3}' \quad \rightarrow \quad \varepsilon^3 v_{i+2}' = \varepsilon^3 v_{i+2}'' + A v_{i+3}' \tag{25}$$

$$m_{i+3} v_{i+3}' = m_{i+3} v_{i+3}'' + m_{i+4} v_{i+4}' \quad \rightarrow \quad A v_{i+3}' = A v_{i+3}'' + \varepsilon^6 v_{i+4}' \tag{26}$$

$$m_{i+4} v_{i+4}' = m_{i+4} v_{i+4}'' + m_{i+5} v_{i+5}' \quad \rightarrow \quad \varepsilon^6 v_{i+4}' = \varepsilon^6 v_{i+4}'' + A v_{i+5}' \tag{27}$$

$$\vdots$$

From the pattern in the previous formulas, equation 23 can be rewritten as $\varepsilon^0 v_i' = \varepsilon^0 v_i' + A v_{i+1}'$. Evaluating the energy conservation equations yields the same form as equations 23–27 except velocities are squared:

$$v_i^2 = v_i'^2 + A v_{i+1}'^2, \tag{28}$$

$$A v_{i+1}'^2 = A v_{i+1}''^2 + \varepsilon^3 v_{i+2}'^2, \tag{29}$$

$$\varepsilon^3 v_{i+2}'^2 = \varepsilon^3 v_{i+2}''^2 + A v_{i+3}'^2, \tag{30}$$

$$Av'^2_{i+3} = Av''^2_{i+3} + \varepsilon^6 v'^2_{i+4}\,, \tag{31}$$

$$\varepsilon^6 v'^2_{i+4} = \varepsilon^6 v''^2_{i+4} + Av'^2_{i+5}\,. \tag{32}$$

$$\vdots$$

We can combine equations 23–27 and 28–32 to eliminate the double-primed terms and form the velocity ratios: $\frac{v'_{i+1}}{v_i}$, $\frac{v'_{i+2}}{v'_{i+1}}$, etc. Beginning with equation 23, we isolate v'_i and square it to obtain $v'^2_i = v_i^2 - 2Av_iv'_{i+1} + A^2v'^2_{i+1}$. Next, substitute this into equation 28 and rearrange to obtain $\frac{v'_{i+1}}{v_i}$. This is then repeated for equation pairs 24 and 29, 25 and 30, etc., to obtain the following ratios:

$$\frac{v'_{i+1}}{v_i} = \frac{2\varepsilon^0}{A+\varepsilon^0}\,, \tag{33}$$

$$\frac{v'_{i+2}}{v'_{i+1}} = \frac{2A}{\varepsilon^3+A}\,, \tag{34}$$

$$\frac{v'_{i+3}}{v'_{i+2}} = \frac{2\varepsilon^3}{A+\varepsilon^3}\,, \tag{35}$$

$$\frac{v'_{i+4}}{v'_{i+3}} = \frac{2A}{\varepsilon^6+A}\,, \tag{36}$$

$$\vdots$$

where we insert a term of ε^0 in equation 33. With our goal being relation 11, we combine equations 33–36:

$$\frac{v'_N}{v_1} = \left(\frac{v'_{i+1}}{v_i}\right)\left(\frac{v'_{i+2}}{v'_{i+1}}\right)\cdots\left(\frac{v'_{N-1}}{v'_{N-2}}\right)\left(\frac{v'_N}{v'_{N-1}}\right) \tag{37}$$

$$= \underbrace{\underbrace{\left(\frac{2\varepsilon^0}{A+\varepsilon^0}\right)\underbrace{\left(\frac{2A}{\varepsilon^3+A}\right)}_{N=3}\left(\frac{2\varepsilon^3}{A+\varepsilon^3}\right)\left(\frac{2A}{\varepsilon^6+A}\right)}_{N=5}\left(\frac{2\varepsilon^6}{A+\varepsilon^6}\right)\left(\frac{2A}{\varepsilon^9+A}\right)}_{N=7} \tag{38}$$

$$\vdots$$

After some observation, the ratio can be put into closed form to obtain

$$\frac{v_N'}{v_1} = \prod_{j=1}^{(N-1)/2} \left(\frac{2\varepsilon^{3(j-1)}}{A+\varepsilon^{3(j-1)}} \right) \left(\frac{2A}{\varepsilon^{3j}+A} \right) \tag{39}$$

$$= 2^{N-1} A^{(N-1)/2} \prod_{j=1}^{(N-1)/2} \left(\frac{\varepsilon^{3(j-1)}}{A+\varepsilon^{3(j-1)}} \right) \left(\frac{1}{\varepsilon^{3j}+A} \right). \tag{40}$$

Turning to the mass ratios, it appears that most terms cancel.

$$\frac{m_N}{m_1} = \left(\frac{m_{i+1}}{m_i} \right) \left(\frac{m_{i+2}}{m_{i+1}} \right) \cdots \left(\frac{m_N}{m_{N-1}} \right) \tag{41}$$

$$= \left(\frac{A}{\varepsilon^0} \right) \left(\frac{\varepsilon^3}{A} \right) \left(\frac{A}{\varepsilon^3} \right) \left(\frac{\varepsilon^6}{A} \right) \cdots, \tag{42}$$

leading to the simple expression

$$\frac{m_N}{m_1} = \varepsilon^{3(N-1)/2}. \tag{43}$$

We can now identify the normalized KE, equation 11, by combining equations 40 and 43 to form

$$KE_N = \left(4A\varepsilon^{3/2} \right)^{(N-1)} \left\{ \prod_{j=1}^{(N-1)/2} \frac{\varepsilon^{3(j-1)}}{\left[A+\varepsilon^{3(j-1)} \right] \left[\varepsilon^{3j}+A \right]} \right\}^2, \tag{44}$$

with $A = f^3 \varepsilon^{3(N-1)/2}$ and $\varepsilon = (1-q)$. This is plotted in figure 5, where it is clear that as f decreases—so that inertial mismatches increase—the normalized KE decays rapidly. Note that the colorscale is calibrated for each subplot.

4. Numerical Solution to the Equations of Motion

A more accurate method of evaluating the dynamics of TCs is to formulate and solve the differential equations of motion (EOM). Given that N is typically small, $\sum F_i = m_i \ddot{z}_i$ can be solved, allowing us to easily keep track of velocities, forces, energies, and positions. The problem will consist of TCs barely touching in their initial configuration and affixed between rigid walls or spheres of infinite radius.

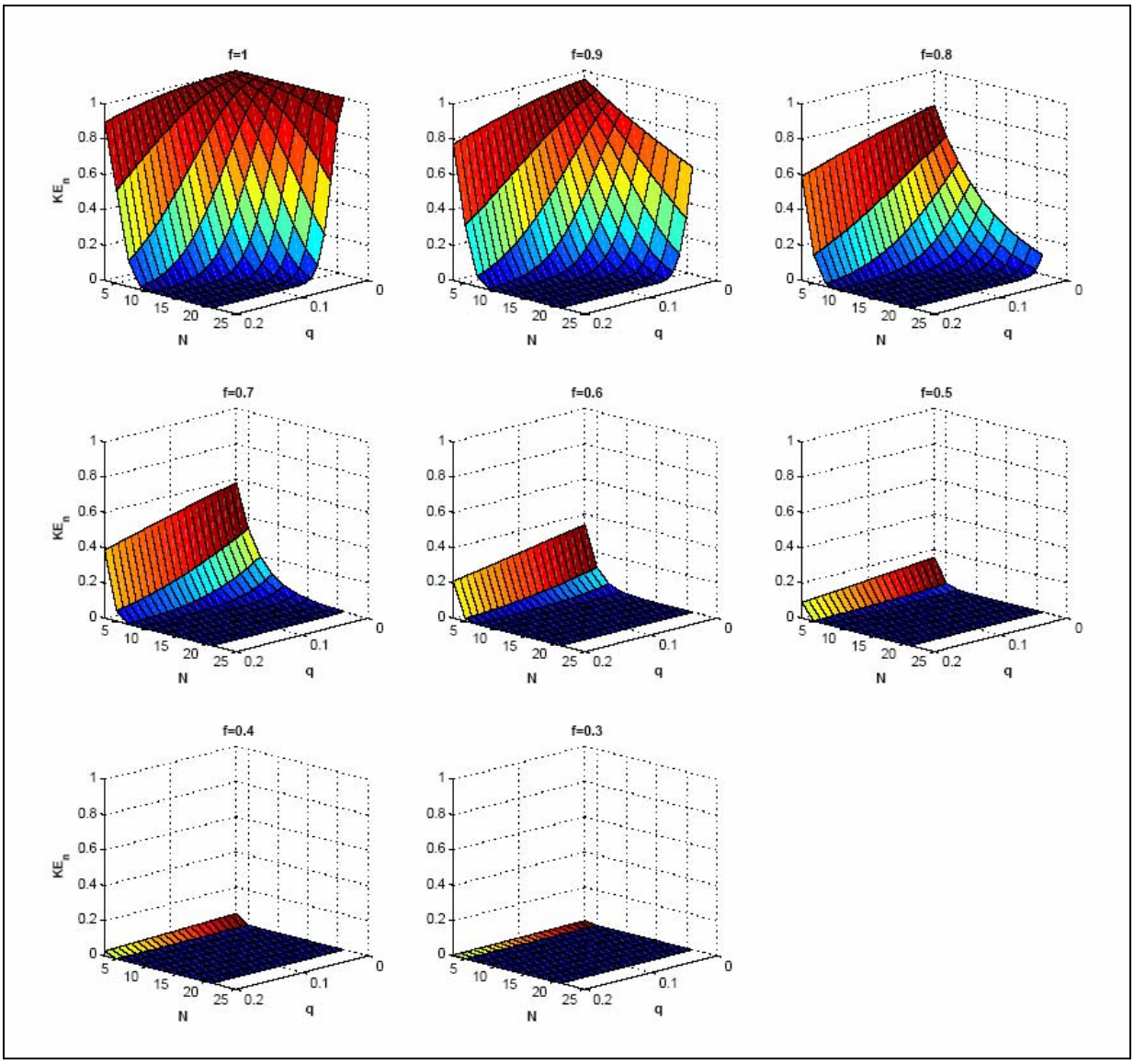


Figure 5. KE as a function of N,q and f for DTC hard-spheres. Note that the colorscale is calibrated for each subplot.

The always-repulsive potential between adjacent grains i and $i+1$ is due to geometric effects and derived in Landau and Lifshitz (*23*). It can be written as

$$V\left(\delta_{i,i+1}\right)=\frac{2}{5D}\sqrt{\frac{R_iR_{i+1}}{R_i+R_{i+1}}}\delta_{i,i+1}^{5/2}\equiv a_{i,i+1}\delta_{i,i+1}^{5/2}, \tag{45}$$

where $R_j : j=\{i,i+1,\cdots,N\}$ are the radii and

$$D=\frac{3}{4}\left(\frac{1-\sigma_i^2}{E_i}+\frac{1-\sigma_{i+1}^2}{E_{i+1}}\right). \tag{46}$$

Here, $\delta_{i,i+1} = R_i + R_{i+1} - (z_{i+1} - z_i)$ represents the overlap between successive grains, where z_j is their position. Additionally, $a_{i,i+1}$ has been defined for material properties: E_j, the Young's modulus and σ_j, the Poisson's ratio; and radii, R_j. Note also that *j* can refer to either particle *i* or $i + 1$. If $\delta_{i,i+1} \le 0$, then $V = 0$ since adjacent grains i and $i+1$ begin to lose contact. For our particular study, all materials are the same in any single TC, so it reduces to

$$D = \frac{3}{2}\left(\frac{1-\sigma^2}{E}\right). \tag{47}$$

Under the Hertzian potential, equation 45, a squeezed sphere initially appears soft. As compression increases, its stillness increases substantially. In this sense, a Hertz potential can be thought of as a nonlinear spring.

At the boundaries, the enclosing walls are represented by spheres of infinite radius: R_0 and R_{N+1}. The corresponding potentials then for grains against the boundary scale as

$V(\delta_{wall,1}) \propto \sqrt{R_1}$ and $V(\delta_{N,wall}) \propto \sqrt{R_N}$.

The force on grain i, therefore, is the sum of influences from its neighboring grains:

$$m_i \ddot{z}_i = \frac{dV}{d\delta} = \frac{5}{2}\left(a_{i-1,i}\delta_{i-1,i}^{3/2} - a_{i,i+1}\delta_{i,i+1}^{3/2}\right). \tag{48}$$

These equations are solved numerically using the Velocity-Verlet algorithm (*27*). The original source code (*8*) which applies to the STC is listed in appendix A. Modifications to this for the DTC are listed in appendix B.

Results have been obtained for a large selection of chains consisting entirely of Ti_6Al_4V or SiC spheres. Arbitrarily, we have chosen to use Ti_6Al_4V when restitutive losses are ignored ($\omega = 0$) and SiC otherwise. The following material properties were assumed (reference D in equation 47).

Table 1. Material properties (*28*).

Material	ρ **(mg/mm^3)**	D **(mm^2/kN)**	**Occurrence**
SiC	3.2	0.003266	$\omega \neq 0$
Ti_6Al_4V	4.42	0.01206	$\omega = 0$

Note that the fundamental unit of force in our simulations is the kilonewton and an initial velocity of 0.01 mm/μs is applied to the largest end of each chain.

Simulations were performed for $3 \le N \le 20$ and $0 \le q, \omega \le 0.1$ over a system time of 1 ms where the timestep was set to 10 ps, corresponding to 10^8 steps in the integration loop.

Restitution, the mechanism for introducing energy losses, is tuned by an asymmetry between the (contact) forces of loading and unloading during a collision:

$$\frac{F_{unloading}}{F_{loading}} = 1 - \omega \ . \tag{49}$$

Therefore, the unloading or expansive force in a collision is some fraction of the loading force and perfectly elastic collisions correspond to $\omega = 0$.

In order to handle the hundreds of TC calculations, a Practical Extraction and Report Language (PERL) script (appendix C) was created to automate the process. It consists of nested loops that iterate through *N* and *q* inserting their new values into a template containing the C code which solves the EOM of the TCs. It then copies this to a directory labeled by some appropriate mnemonic. This was done so that when visualizing the data in MATLAB, it would be easy to change directories as part of a loop. An example directory structure is, `/w0/N20/N20q10/taperchain1.cpp`. Data files are created for every grain in each TC and their number is encapsulated in the filename. Appendix D contains the MATLAB code to generate KE surfaces.

Recall that we are interested in forming the ratio $KE_N = KE_{out}/KE_{in}$, the normalized KE. Here, KE_{out} is the first* kinetic energy peak felt by the last (smallest) grain and KE_{in} is a constant determined from the initial velocity and density of the first grain. Conversely, F_{out} is the first minimum felt by the last grain since the direction of a negative force is into the wall or force sensor. The algorithm to pick out the first turning point for each of these is straightforward. Since $KE(t)$ is a column vector, one can iterate through each element until the first occurrence of $(i+1) < i$ is true. In that case, i represents the extremum. For force, we compare against $(i+1) > i$. The only data files then that are of interest for KE_N are those that represent the dynamics of the first (KE_{in}) and last particle (KE_{out}) in each chain.

4.1 STC

Figure 6 plots a small cross section of the results for several chains with $N = 20$, $\omega = 0.05$, and $q = \{0,\ 0.02,\ 0.04,\ 0.06,\ 0.08,\ 0.1\}$. These plots show the kinetic energy spectrum of the tail particle as a function of time for the first half of the simulation (500 μs). From equation 49, each collision only transmits 95% of the force. Note the decreasing scale of KE in each underlying panel. One might expect KE to increase since particle velocity is increasing. However, KE scales as v^2 and $m \propto r^3 \propto (1-q)^3$, so the latter term dominates, and consequently KE decreases.

In the top panel of figure 6, we see at about 95 μs that the tail particle in a monodisperse chain first receives the energy bundle and undergoes translational motion. Its contact force with the

* Normalization is discussed further in appendix E.

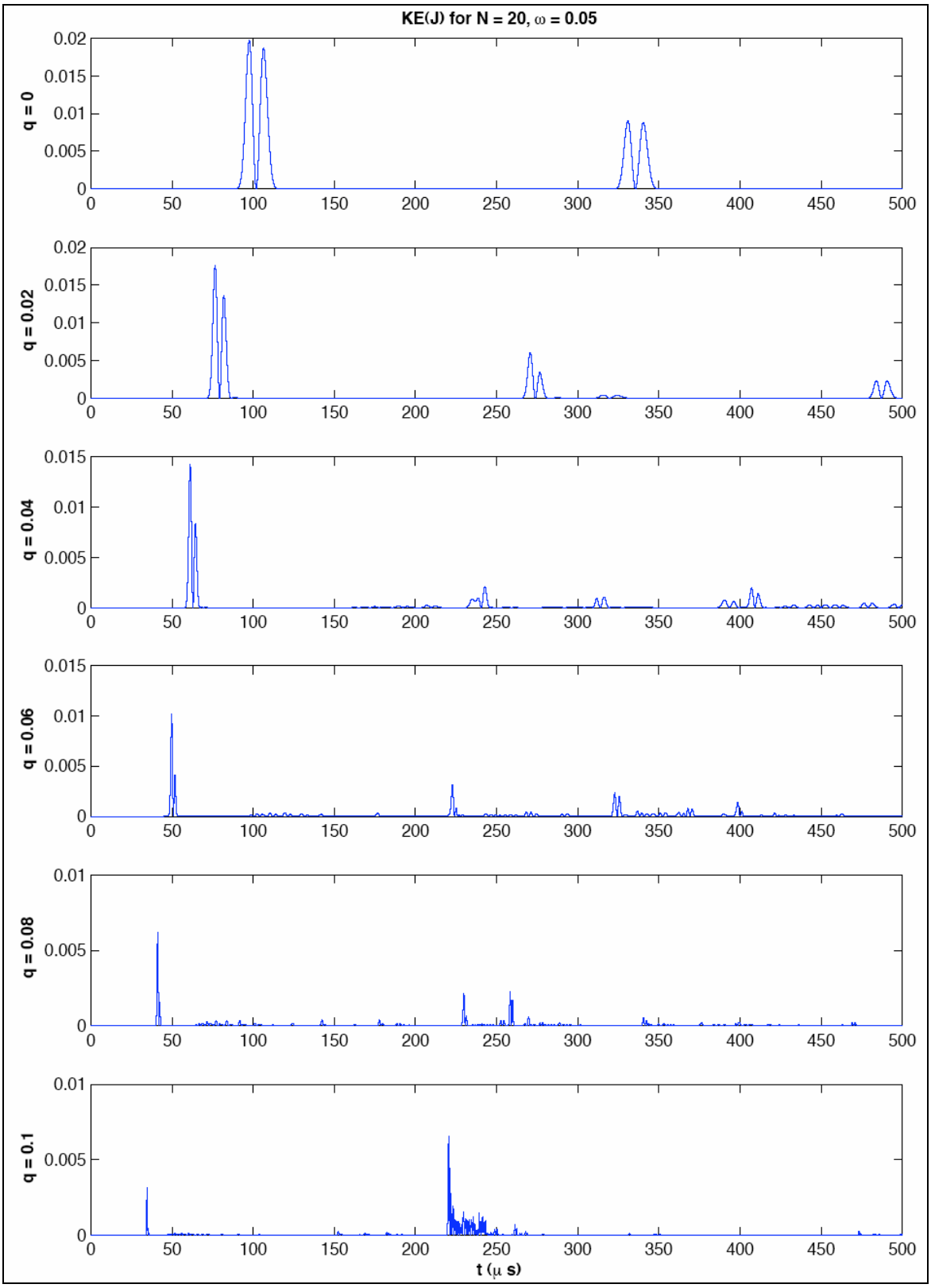


Figure 6. KE as a function of time for the smallest particle in a chain with $N = 20,\ \omega = 0.05,$ and $q = [0 : 0.02 : 0.1]$. Each plot is evaluated for a different tapering with initial KE as 0.0838 J.

boundary increases as it slows down eventually coming to rest with all energy stored as elastic potential at about 100 μs. This is then converted back to kinetic as the tail particles begin to rebound.

By selecting the first peak in each of these subplots as well as the many other chains not shown here, we can form the normalized KE surfaces and observe how well STCs perform as energy absorbers.

Pulses in monodisperse chains ($N \geq 15,\ q = 0$) represent a special class of waves known as a solitary waves which are remarkably stable and have been studied extensively (*2–7*, *9*, *11–12*). For TCs ($q \neq 0$), the solitary wave cannot quite fully form because subsequent grains within the wave envelope move at higher, disparate velocities with increasing q—leading to greater dispersion and destructive wave broadening. This translational symmetry breaking was also reported by and is in agreement with Nakagawa et al. (*4*).

4.1.1 STC KE and Force Parameter Spaces: $KE(N,q,\omega), F(N,q,\omega)$

Figure 7 highlights the numerical results for *KE*(*N*, *q*, constant ω). Note that it would be very difficult and costly to produce a similar plot empirically. Each node on the surface represents a different TC and experiment. There appears to be a sigmoidal and exponential dependence on q and N, respectively, in agreement with the hard-sphere approximation. These KE surfaces represent STC chains that thermalize more than half the incident energy introduced into the system. For example, the least effective shock mitigating geometry that we've simulated here—*KE*(ω = 0, N = 3, q = 0)—reduces the output KE by about 60%. That amount, after restitution is accounted for in cases where $\omega \neq 0$, is distributed among the other grains as kinetic and potential energy. Note again that results are independent of initial grain size. For monodisperse chains ($q = 0$) in figure 7a, there is asymptotic behavior as N increases which is a result of energy propagating as solitary waves, when N is of sufficient number (about 15), energy can propagate with negligible loss. Additionally, there is a rapid drop in *KE*($3 \leq N \leq 5$, q = 0, ω = 0) which is likely due to the width of the incident pulse being longer than the TC. This implies that wave reflection begins before the impulse is fully applied.

A similar surface can be plotted representing the normalized force for various TCs. This is visible in figure 8 and similar to the KE plots. Again, the functionality of N here is essentially a one to two phase exponential, but the sigmoidal nature of q is less obvious and can be approximated linearly throughout the parameter space. In general, the magnitude of F appears to be twice that of KE.

The numerical results can be compared to the hard-sphere approximation by scaling the latter to the largest numerical solution—KE ($N = 3,\ q = 0$)—and plotting their difference (figure 9). Energy loss is not accounted for in this comparison. The distribution is due to differences in the interaction potential and width of the energy bundle. Therefore, it appears that for smaller particles (i.e., larger q) compressive effects and width of the energy packet becomes increasingly important. This is compounded further by increasing the number of particles, N.

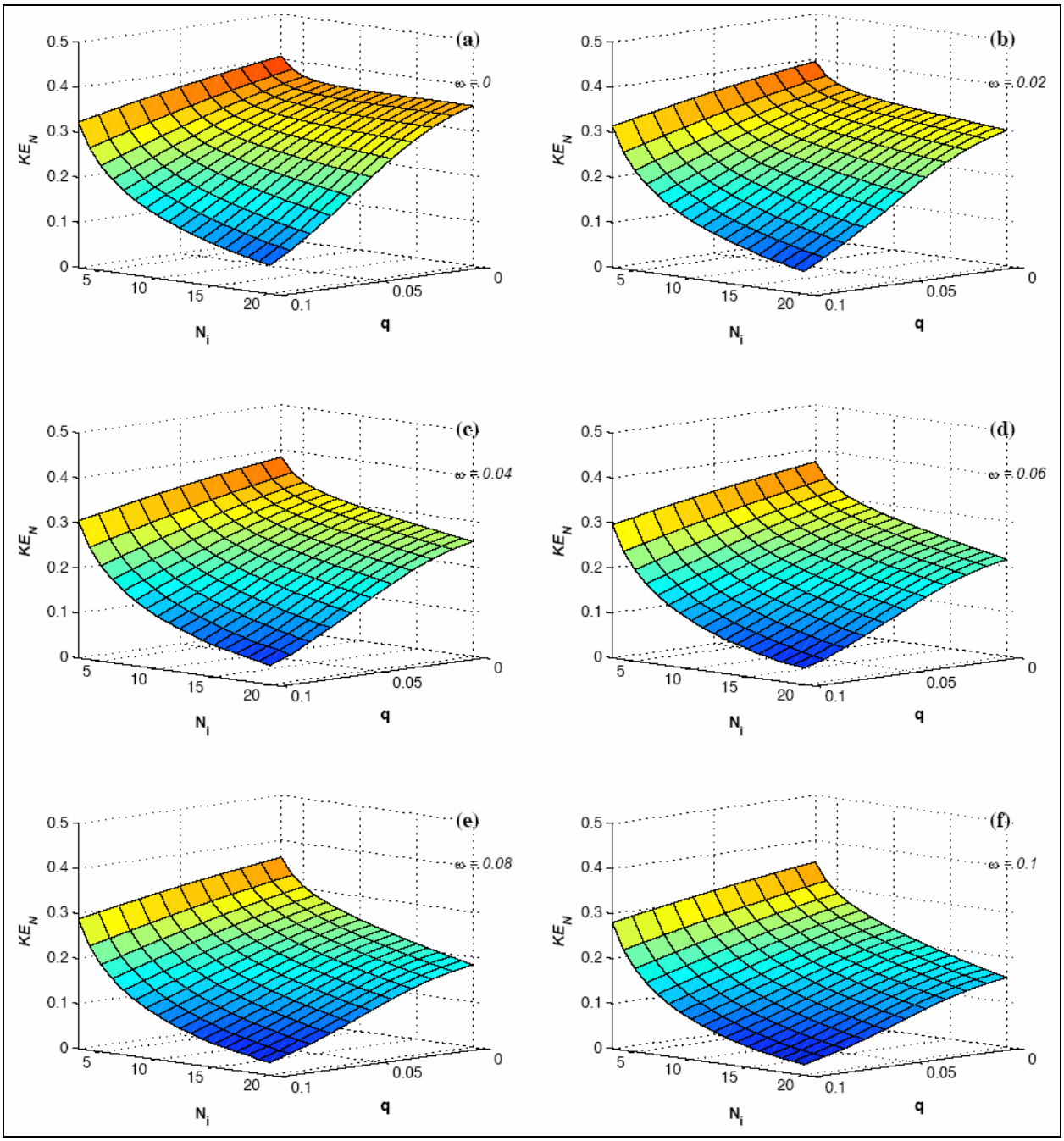


Figure 7. Numerical solution of $KE(N,q)$ parameter space for constant ω. Note that it would be very difficult and costly to produce a similar plot empirically. Each node on the surface represents a different TC and experiment.

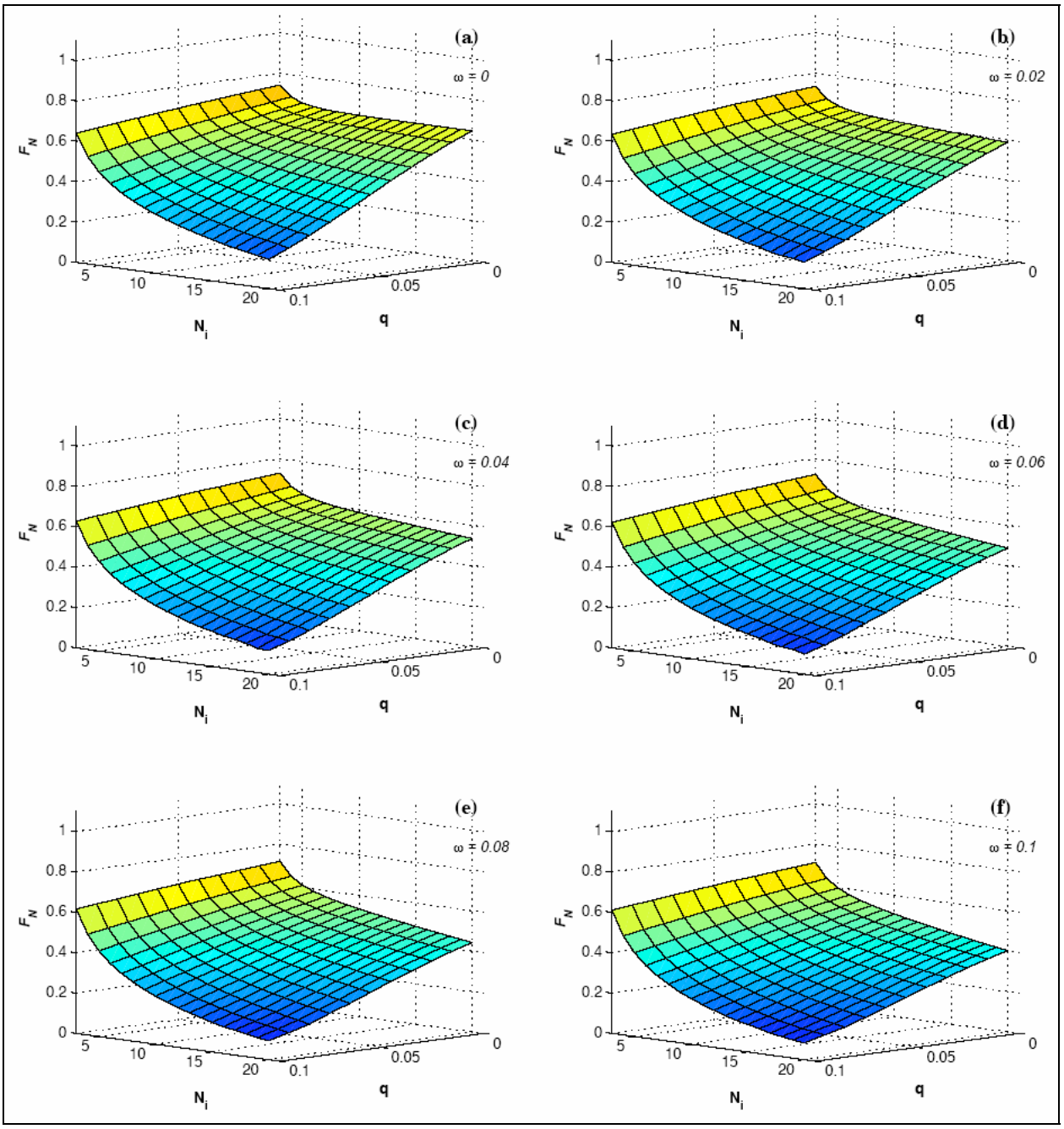


Figure 8. Numerical solution of $F(N,q)$ parameter space for constant ω.

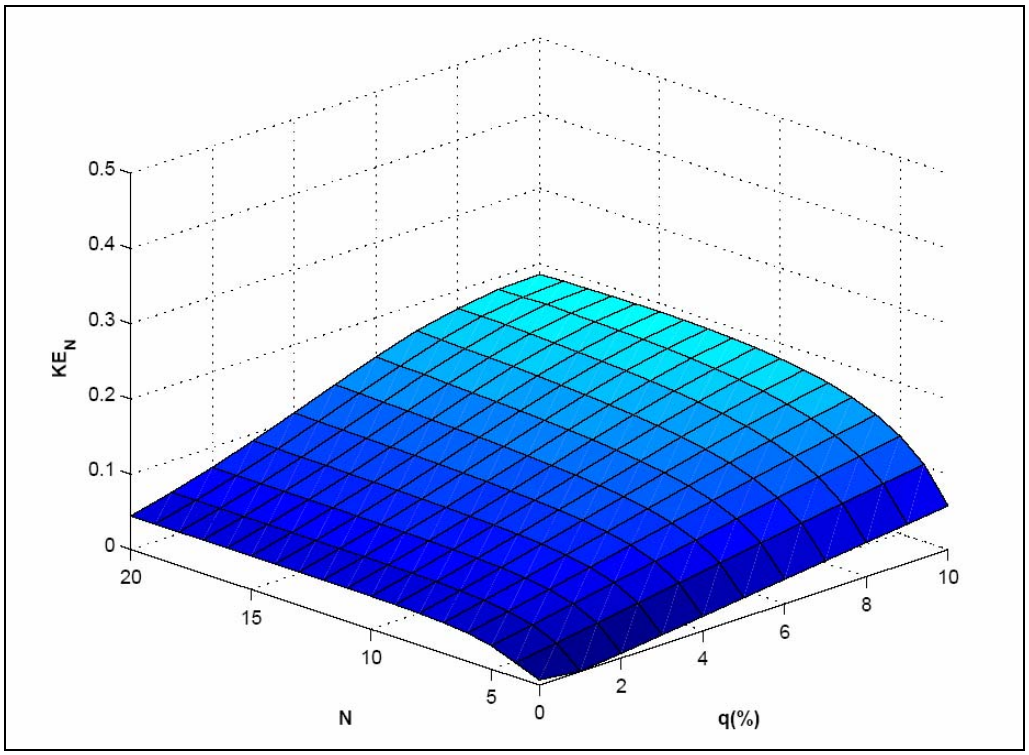


Figure 9. Difference plot of the lossless KE parameter spaces for the hard-sphere approximation (figure 2a) and numerical solution (7a). Note that the azimuthal view has been rotated 180° for clarity.

4.1.2 STC Mathematical Model

It would be convenient to have a predictive capability for at least a selection of individual TCs as a function of N, q, and ω. We therefore propose a mathematical model for the $KE = KE(\omega, q, N = 20)$ parameter space of the form

$$KE(\omega, q) = Ae^{Bq^C} e^{D\omega^E}, \tag{50}$$

which corresponds to a two-dimensional Weibull distribution. One can obtain the sigmoidal and exponential behavior of q and ω, respectively, when the exponents are restricted to $C > 1$ and $E \leq 1$. For simplicity, we set $E = 1$ and $C = 3/2$ since these values provide the general functionality. The coefficients B and D were evaluated using 4th-order polynomial fits and the scaling coefficient A is essentially the point $KE(N = 20, \omega = q = 0)$ determined in the simulation. It turns out that a 2nd-order fit was not sufficiently robust and a higher-order fit yielded marginal gains at the cost of mathematical encumbrance.

This model currently lacks the rigor sufficient for planar behavior in the limit of small N. It is unclear at this point if N can be completely decoupled from ω and q and written as an additional exponential term. In all likelihood, the coefficients B and D would be written as functions of N.

Ultimately, it would be useful to expand equation 50 and have a model that completely describes the normalized KE as a function of N, q, ω, and Δ where the latter is a constant external loading or precompression of the chain.

In evaluating the fits, we find that $KE(\omega,\ q,\ N=20)$ is described quite well by

$$KE(\omega,q) = 0.35544 \cdot e^{\left(\left[-1.5055\cdot10^{-5}q^4+4.016\cdot10^{-4}q^3-3.981\cdot10^{-3}q^2+0.0147q-0.05435\right]q^{3/2}\right)} \cdot \cdot e^{\left(\left[4.144\cdot10^{-5}q^4+1.955\cdot10^{-3}q^3-0.03962q^2+0.02887q-8.341\right]\omega\right)} \tag{51}$$

It is compelling to rewrite equation 51 in the more suggestive form

$$KE(\omega,q) \propto e^{\alpha q^{11/2}} e^{\beta q^{9/2}} e^{\gamma q^{7/2}} e^{\delta q^{5/2}} e^{\varepsilon q^{3/2}} \cdots \tag{52}$$

$$\propto e^{\alpha q^{(n+3)}} e^{\beta q^{(n+2)}} e^{\gamma q^{(n+1)}} e^{\delta q^{n}} e^{\varepsilon q^{(n-1)}} \cdots \tag{53}$$

where the powers of q have been adjusted to be written as a series in n, the interaction potential—equivalent to 2.5 for Hertzian spheres. The occurrence of an apparent series in n is quite striking. Missing from this of course is a $(n-2)$ or $q^{1/2}$ term which requires a different fit for B in equation 50. Note also the mixed term $q\omega$ in equation 51. This is indicative of a many-body effect; one cannot have restitution in a single particle chain since, by definition, it requires at least two to evaluate the loading and unloading.

Figure 10 compares the numerical results and the model for the case of $N = 20$. The results are practically indistinguishable except for minor timestep errors in the simulation which appear as noise for large q. At these values for N and q, the tail particle has a large velocity and for timesteps not small enough, the KE plots lose their smoothness. The algorithm therefore selects a peak close to what the real extremum would be in the limit that the timestep approaches zero. As such, the model is more accurate.

4.2 DTC

In this section, we address the more capable DTC. KE time spectra is excluded since an analysis of the complicated motion is outside the scope of this report. Instead, let us focus immediately on the KE parameter space and compare with the STC.

Figure 11 illustrates the intriguing nature of the DTC $KE(N,q,f)$ surfaces where the dissimilarity from the DTC hard-sphere approximation is quite clear. Immediately obvious is a ripple across the surface for large f which translates towards the origin as f decreases. The effect vanishes at about $f = 0.6$ and the KE surface resembles that of a much-improved STC for $f \le 0.5$. We propose qualitatively that this is a consequence of the inertial mismatch changing as a function of position in the DTC—in contrast to the STC where it is constant along the chain and the wave effect is not observed.

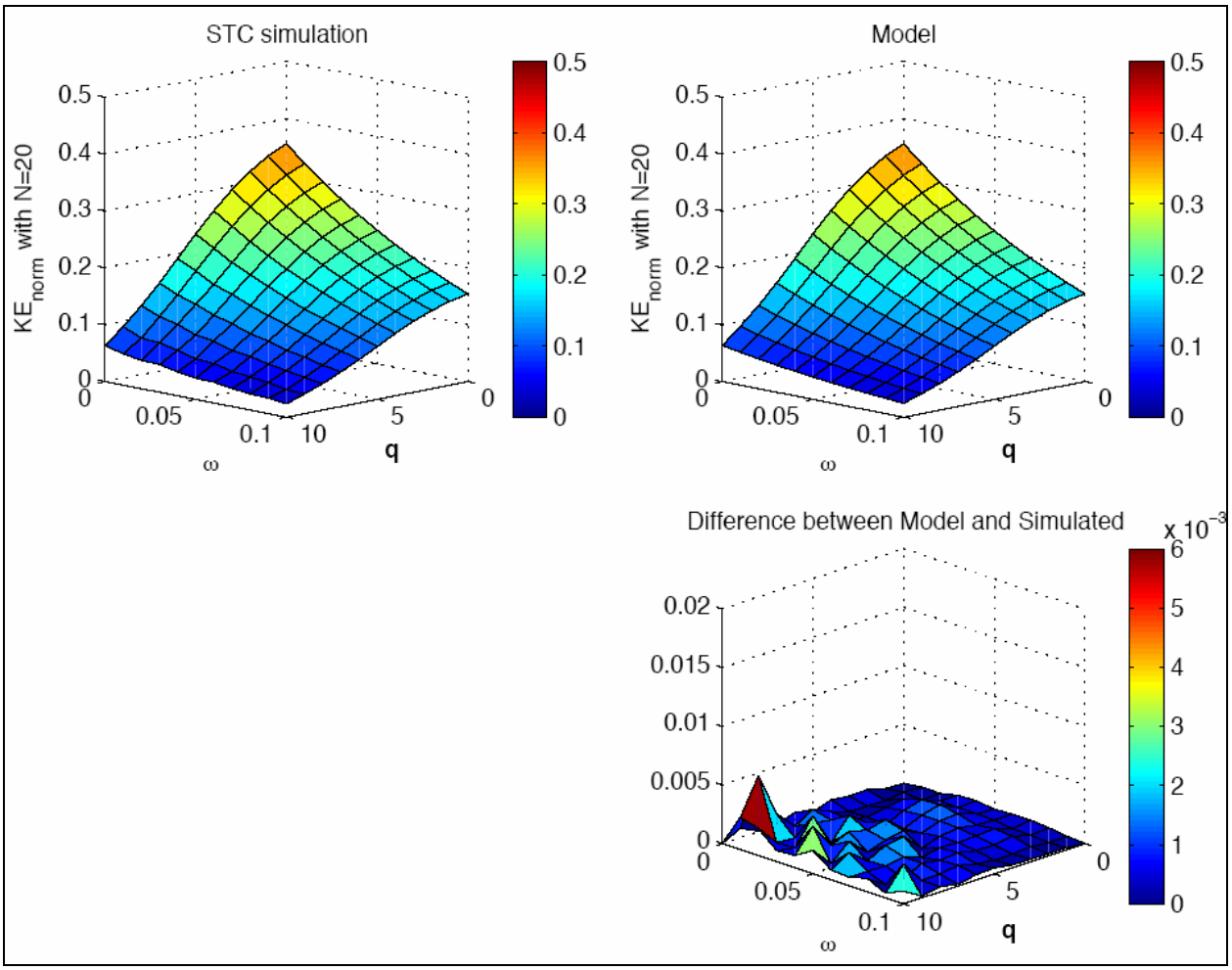


Figure 10. The simulated and modeled STC.

In the side panel in figure 11, several DTCs are shown. In the top case, $f = 1$, so that as the incident pulse propagates to the left, the chain becomes increasingly monodisperse. That degree of monodispersity is a function of N and q since wave amplitude and velocity is sensitive to them. If N is large enough, then whatever remaining energy is left could propagate nearly lossless like a solitary wave. As f gets smaller (next panel down), any apparent monodispersity begins to disappear. As one moves to the right in the chain, the interstitial grains become small compared to the neighboring grains. As f becomes smaller still, the interstitial grain is small compared to all grains such that reducing f has little effect—little enough so that the wave behavior on the KE surface is not observed. Thus there appears to be a transition so that when $f \leq 0.5$, the chain will never appear monodisperse and inertial mismatches can always be considered large.

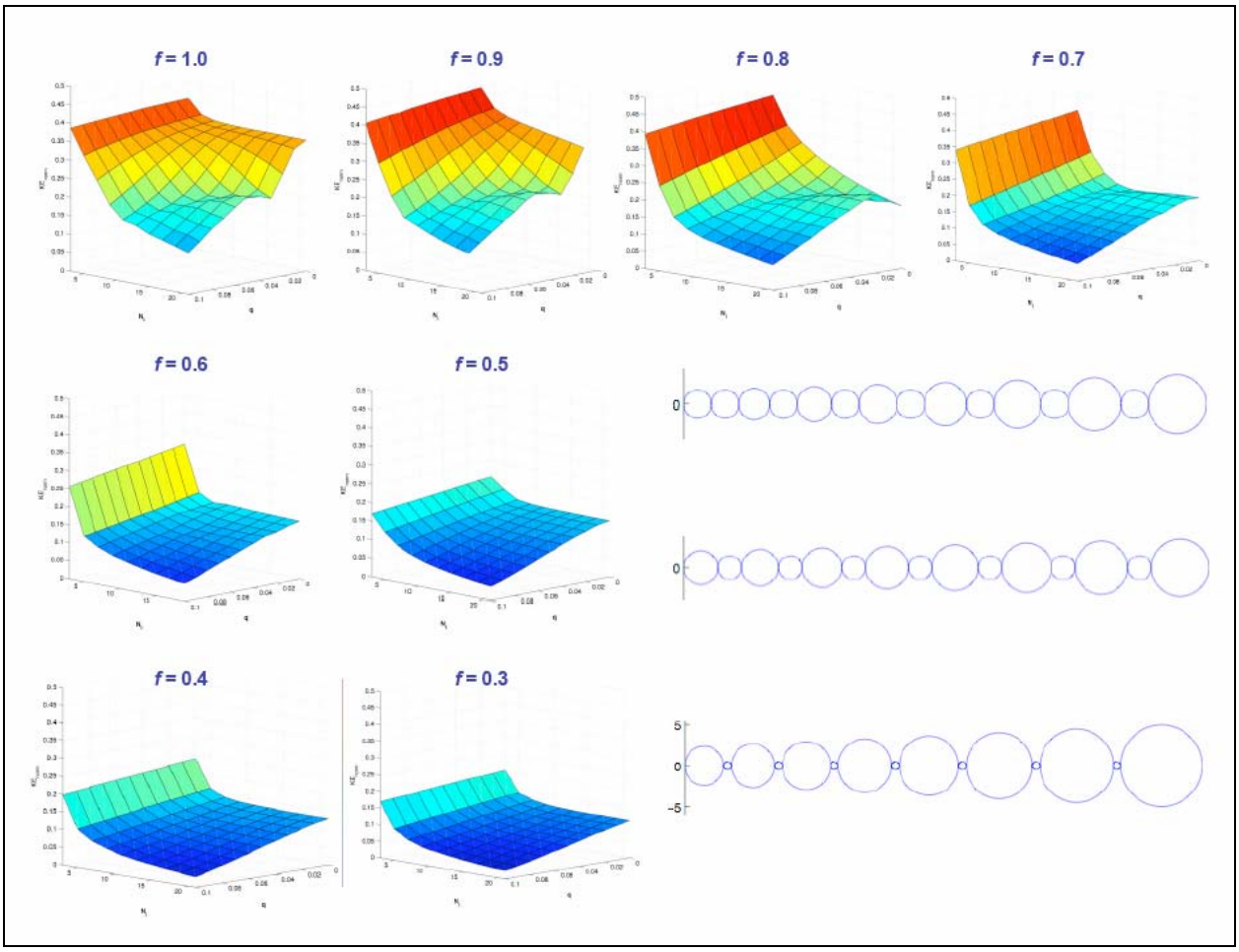


Figure 11. DTC numerical solution of $KE(N,q,f)$ and sample DTCs for various f (inset). The scale is the same as that in figure 7.

5. Experimental Efforts

Up to this point, most experimental work reported in the open literature has focused on monodisperse chains by themselves or as a precursor to TCs. Here we only discuss the setup used in such studies as well as the prototype for our intended investigation of the DTC.

5.1 STC

There are two common ways of performing STC experiments. The first (*11*) is based on a Newton's cradle but more epic in extent (figure 12). In this particular case, there is a monodisperse sequence used to set up a well-defined solitary wave which propagates to the left. A small striking sphere on the far right is applied to generate the initial pulse.

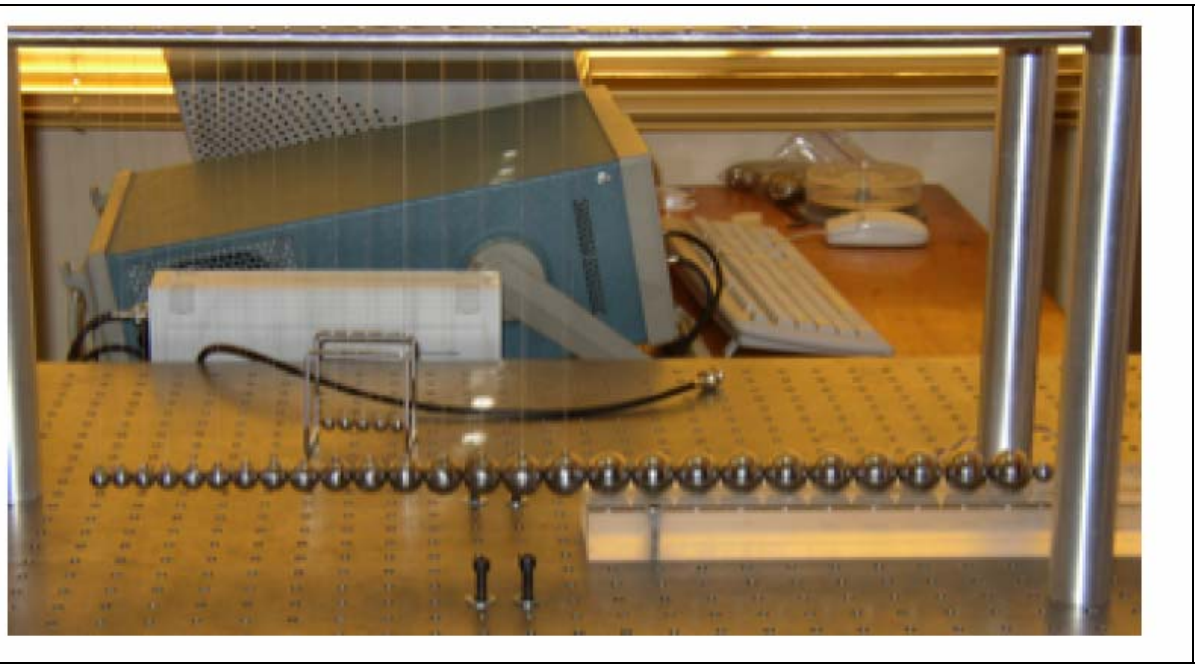


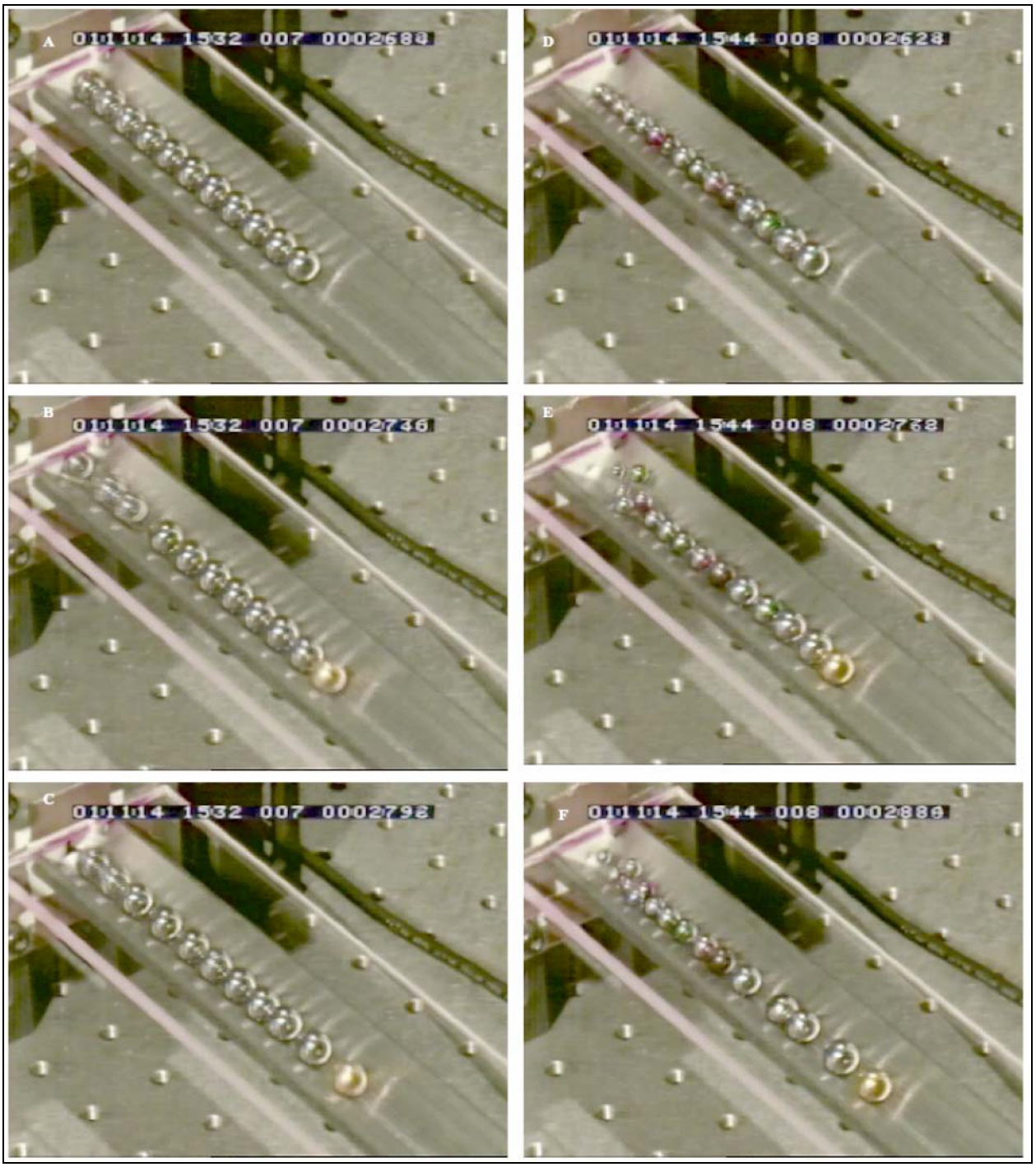
Figure 12. STC experimental setup by Job et al. (*12*).

The second common STC configuration (*4*) consists of a V-shaped track which can be slanted to ensure proper (centerline) contact of the tapered spheres (figure 13). Here, the left column highlights a monodisperse chain and the right column shows the same experiment but for a TC—subsequent rows represent later time. In the middle row, the striker (gold sphere) has hit the chain; in the bottom row, the tail particle in the monodisperse chain has perforated the paper target (black hole in upper left of picture), while for the TC on the right, it merely dents and bounces off the paper. This is a remarkable demonstration of the impulse decimation capability inherent to TCs.

5.2 DTC

Figures 14–16 highlight the constituents and current housing of a DTC configuration.

Within the assembly, interstitial grains are radially constrained along the axis of the DTC by thin discs with small holes bored in them (figure 16). The apparatus can be tested in any orientation; however, when vertical, asymmetric loading due to gravity will become a factor. Uniform precompression enhances the shock absorption capability of TCs and will be discussed in the next section. In figure 15, we see that precompression of the DTC prototype can be controlled by the large screw at the top of the assembly.



Source: Picture courtesy of Prof. M. Nakagawa of the Colorado School of Mines and Dr. Juan Agui of the National Aeronautics and Space Administration–Glenn Research Center.

Figure 13. STC experimental setup. The left half of the figure represents a monodisperse chain while the right a TC. Lower plots denote later time.



Figure 14. Preliminary DTC housing chamber.



Figure 15. DTC constituents.



Figure 16. DTC interstitial grains.

6. Precompressed Chains

Apparently, when TCs are precompressed, shock absorption increases substantially (*3*). We measure precompression, Δ, as a percentage of particle overlap in the initial state. The EOM in equation 48 are modified accordingly and become

$$m_i \ddot{z}_i = \frac{5}{2}\left\{a_{i-1,i}\left[R_{i-1}+R_i-\Delta-\left(z_i-z_{i-1}\right)\right]^{3/2}-a_{i,i+1}\left[R_i+R_{i+1}-\Delta-\left(z_{i+1}-z_i\right)\right]^{3/2}\right\}. \qquad (54)$$

Figure 17 highlights the impressive results for $KE\left(N=20,\ \Delta=0.03\%\right)$ as tapering and restitution are varied. Precompression in a DTC could therefore provide the best shock absorption geometry that we have currently considered.

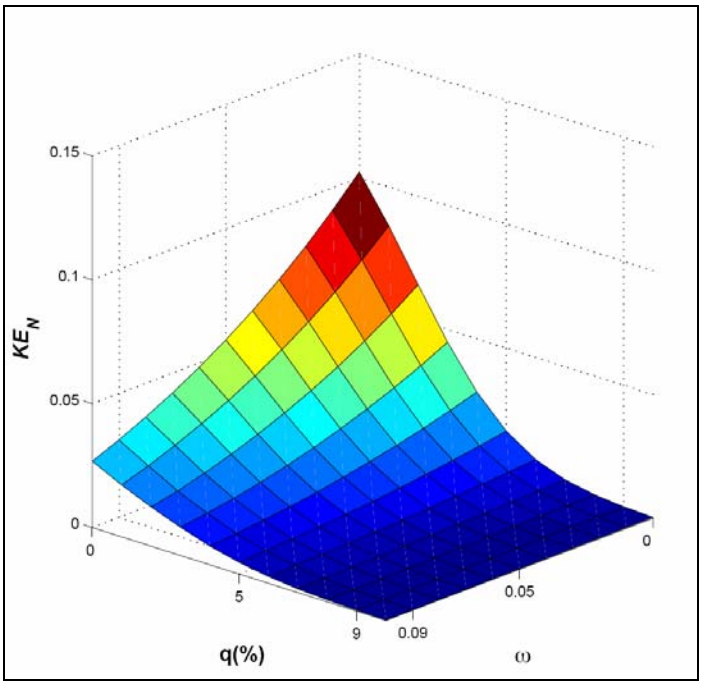


Figure 17. KE as a function of tapering and restitution for constant $N = 20$ and $\Delta = 0.03\%$.

7. TC Armor Panels

We have seen that Hertzian TCs act as shock absorbers. In particular, recall that at the end of section 3.1.3 we noted that TCs operate regardless of a pulse's direction through the chain. Thus, to maximize efficiency, we can place neighboring STCs in alternating directions.

For them to become realizable in armor applications, however, one should evaluate them based on performance of the whole system. The specific absorbed energy (SAE)—which has units of J/g—is one such metric and commonly used by ballisticians. It is quantified by equation 55, while the volumetric absorbed energy (VAE) is described by equation 56 and has units of J/cm^3.

$$\frac{\left|KE_{in} - KE_{out}\right|}{M} = \frac{\left(1 - \frac{KE_{out}}{KE_{in}}\right) KE_{in}}{M} = \frac{\left|1 - KE\left(N, q, \omega\right)\right| KE_{in}}{M}. \tag{55}$$

$$\frac{\left|1 - KE\left(N, q, \omega\right)\right| KE_{in}}{V}. \tag{56}$$

Here, $KE(N,q,\omega)$ is the normalized KE that has been evaluated in the numerical simulations. Figure 18 illustrates what a TC armor prototype might resemble along with an incident flyer plate.

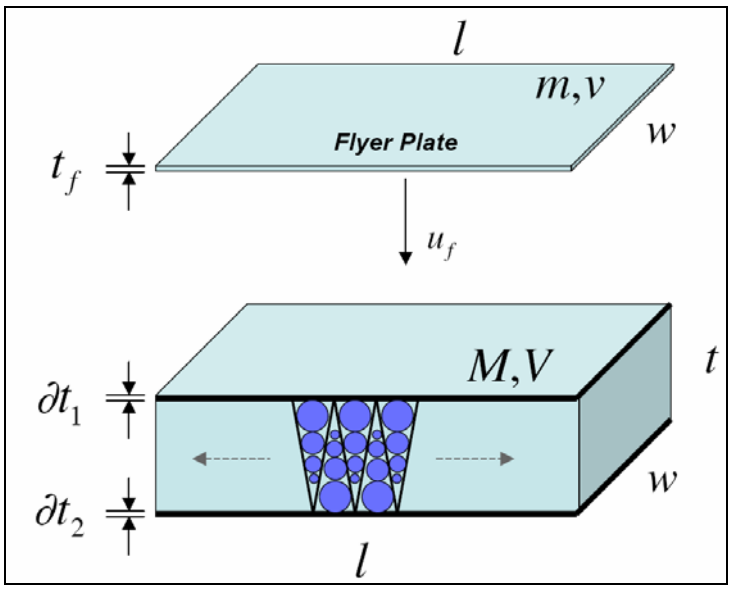


Figure 18. STC armor plate panel.

In equations 55 and 56, KE_{in} represents the energy of the incoming flyer plate. For convenience, we assume that all materials are Ti_6Al_4V ($\rho = 4.42$ mg/mm^3), that u_f= 100 m/s, t_f= 24.5 mm, and that $l = w = 230$ mm. Since $m = \rho V = \rho l w t_f$, the KE of the flyer plate, KE_{in}, is 28.7 kJ. Also, in both cases, we set $KE(N,q,\omega) = KE(20,0.1,0.06) \approx 0.05$, which is obtained from the numerical results. Thus, the sizes of the end spheres in such a chain are $d_{20} = 10$ mm and $d_1 = 1.35$ mm.

In order to evaluate M in equation 55, several assumptions are made and then later relaxed to determine a range for M and better approximate what type of performance a TC armor panel might achieve. Figure 18 displays the relevant variables and configuration for a preliminary analysis, where $t = 95.8$ mm is chosen based on the chain parameters used in picking $KE(N,q,\omega)$.

Each STC would require some type of mechanical support to maintain the overall geometry. One solution is to house them in hollow cones as is displayed in the diagram. Conical springs, or Belville washers, are another possibility. We can absorb this added material into d_1 as an effective diameter which we set to $\tilde{d}_1 = 1.5$ mm. The additional dimensions, w, l, are arbitrarily assigned to be a function of the number of TCs: $l = w = 20(d_{20} + \tilde{d}_1) = 230$mm, so that each side is spanned by 40 TCs. Therefore, the total number of TCs in the armored panel is 1600. Finally,

$\delta t_1, \delta t_2$ represent thicknesses for enclosing plates so that the TCs aren't exposed. This amount is arbitrary but chosen to be small, $\delta t_1 = \delta t_2 = 2.5$ mm, so that the total thickness of the panel is 100.8 mm, or about 4 in.

Now, M can be written as the sum, $M = N_{\text{STC}} m_{\text{STC}} + 2m_{\delta t} + m_{\text{support}} + m_{\text{fill}}$, where the first term is the product of the mass of one STC and the total number of them, the second is the contribution from the enclosing plates, the third is due to the conical housing of STCs, and the last is the filler material which we ignore as being air. Using conservative values, we let $m_{\delta t} = (\delta t) lw\rho = 0.58$ kg, $m_{\text{support}} = 1.0$ kg so that $M = 13.63$ kg.

Since equation 55 scales with u_f, the velocity of the flyer plate, a wide range of SAE can be determined. If $u_f = 100$ m/s, the SAE=2. Let us assume then that $6.63 \le M \le 20.63$ and $100 \le u_f \le 300$ m/s and plot the SAE surface which is visible in figure 19a.

The VAE can be calculated by dividing this quantity by the density of the material—since we are assuming the whole panel is Ti_6Al_4V (figure 19b). Another measure, however, would be to divide by the volume of the entire panel since that space is already claimed and cannot be occupied by anything else. In dividing by the density, we are only counting that portion of the armor panel contained by Ti_6Al_4V; it doesn't include the air fills. Note that the SAE and VAE have been determined primarily analytically.

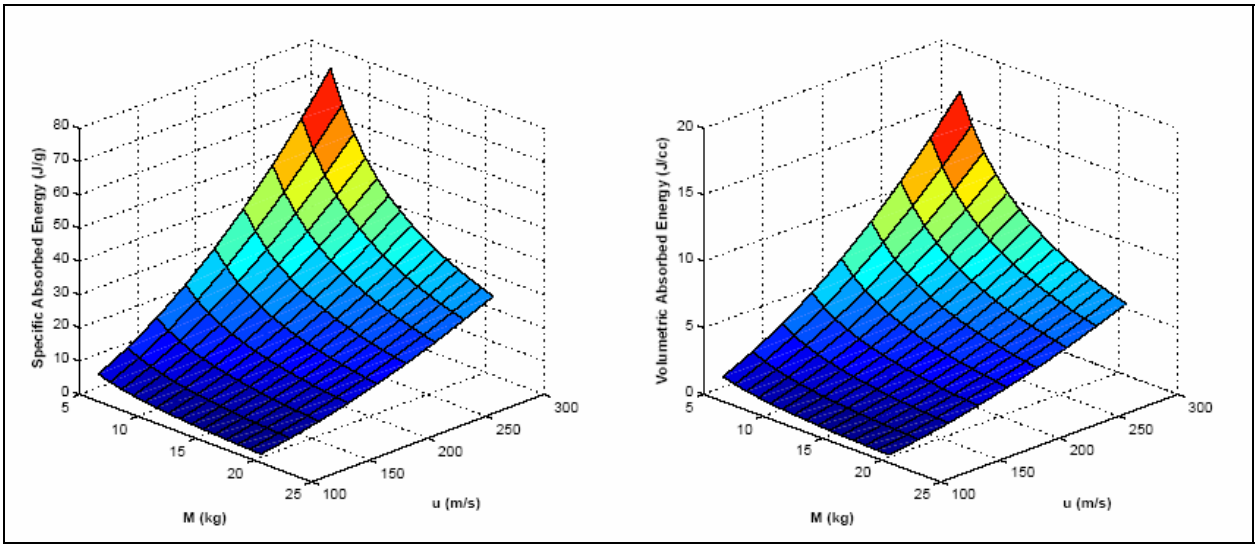


Figure 19. SAE and VAE as a function of M, the total STC armor panel mass, and u_f, the incident flyer plate velocity.

8. Concluding Remarks

This report has focused on TCs and their inherent ability to decimate propagaing impulses. Due to a lack of dependence on system size, it appears that TCs can provide meter to submicron scale shock absorption. TCs take well-defined pulses, such as shocks, and turn them into noise. The signal is spread out over time and space and the process is known as thermalizing an impulse (*3*).

Essentially, the shock is stretched from a few microseconds to several hundred with its extent increasing from several grains to all members in the TC. This is in opposition to monodisperse chains which act as highly efficient shock transmitters due to the resilient nature of solitary waves. In fact, Pöschel and Brilliantov have calculated (*29*) the optimal transmission of KE for TCs.

It turns out that regardless of whether an impulse travels forwards or backwards along a chain, both directions mitigate a propagating pulse. At later times, this likely competes with coordinated motion of adjacent grains which may create unpredictable energy or force spikes for certain configurations, as figure 7 (lower panel) demonstrates. Antiparallel orientations of TCs can then be arranged to exploit the collective effects of many TCs as an armor panel. The capabliity of such a panel is analytically derived and yields values for the SAE on the same order 10^0-10^2 J/g as other technologies. However, such a determination is still rather suggestive without a full scale prototype. TCs may be housed in hollow cones or Belville washers (conical springs) for added absorption. Additionally, there is evidence (*30*) that nitinol (a nickel-titanium alloy) may be a better material to choose for the spheres and housing.

Hard-sphere approximations were analytically obtained for two chain geometries, the STC and DTC. This approximation simplifies the problem to one where the impulse delivered is a single grain in width and elastic effects are ignored. For the STC, this approximation is comparable to the numerical results. However, for the DTC, the differences are quite large and consequently elastic effects play a major role in the system. This is likely due to the increased velocity of members in the chain and therefore the number of collisions.

The authors see ample opportunity for study along several lines to move this technology forward and rate it as a useful technology in blast mitigation system. Quasistatic compression to plasticity and failure, ALEGRA simulations, and measuring the effects of many TCs working in cooperation are areas we are beginning to investigate.

9. References

1. Doney, R.; Sen, S. The Tapered Chain: Hard Sphere Approximation and Simulation. *Phys. Rev. E*., submitted for publication, July 2005.
2. Sokolow, A.; Pfannes, J. M. M.; Doney, R.; Nakagawa, M.; Agui, J. H.; Sen, S. Impulse Absorption by Small Tapered Granular Chains. *Science*, submitted for publication, 2005.
3. Sen, S.; Manciu, M. Thermalizing an Impulse. *Phys. A* **2001**, *299*, 551–558.
4. Nakagawa, M.; Agui, J.; Wu, D. T.; Extramiana, D. V. Impulse Dispersion in a Tapered Granular Chain. *Gran. Mat*. **2003**, *4*, 167–174.
5. Wu, D. Conservation Principles in Solitary Impulse Propagation Through Granular Chains. *Phys. A* **2002**, *315*, 194–202.
6. Manciu, M.; Sen, S.; Hurd, A. J. The Propagation and Backscattering of Soliton-Like Pulses in a Chain of Quartz Beads and Related Problems (I). *Propagation. Phys. A* **1999**, *274*, 588–606.
7. Manciu, M.; Sen, S.; Hurd, A. J. The Propagation and Backscattering of Soliton-Like Pulses in a Chain of Quartz Beads and Related Problems (II). *Backscattering. Phys. A* **1999**, *274*, 607–618.
8. Pfannes, J. Energy Propagation in Granular Chains. M.S. Thesis, State University of New York, Buffalo, NY, May 2003.
9. Coste, C.; Falcon, E.; Fauve, S. Solitary Waves in a Chain of Beads Under Hertz Contact. *Phys. Rev. E* **1997**, *56* (5), 6104–6117.
10. Rossmanith, H. P.; Shukla, A. Photoelastic Investigation of Dynamic Load Transfer in Granular Media. *Acta Mech*. **1982**, *42*, 211–225.
11. Sen, S.; Manciu, M.; Wright, J. D. Solitonlike Pulses in Perturbed and Driven Hertzian Chains and Their Possible Applications in Detecting Buried Impurities. *Phys. Rev. E* **1998**, *57* (2), 2386–2397.
12. Job, S.; Melo, F.; Sokolow, A.; Sen, S. How Hertzian Solitary Waves Interact with Boundaries in a 1D Granular Medium. *Phys. Rev. Let*. **2005**, *94* (178002), 1–4.
13. Duran, J. *Sands, Powders, and Grains*; Springer-Verlag: New York, NY, 2000.
14. Mehta, A., Ed. *Granular Matter*; Springer-Verlag: New York, NY, 1994.

15. Kakalios, J. Resource Letter GP-1: Granular Physics or Nonlinear Dynamics in a Sandbox. *Am. J. Phys*. **2005**, *73* (1), 8–22.

16. Jaeger, H. M.; Nagel, R. Physics of the Granular State. *Science* **1992**, *255* (5051), 1523–1531.

17. Jaeger, H. M.; Nagel, R.; Behringer, R. P. Granular Solids, Liquids, and Gases. *Rev. Mod. Phys*. **1996**, *68* (4), 1259–1273.

18. Wright, T. *Weak Shocks and Steady Waves in a Nonlinear Elastic Rod or Granular Material*; BRL-TR-02584; U.S. Army Ballistics Research Laboratory: Aberdeen Proving Grounds, MD, 1984.

19. Walton, O. R.; Braun, R. L. Viscosity, Granular-Temperature, and Stress Calculations for Shearing Assemblies of Inelastic, Frictional Disks. *J. Rheol*. **1986**, *30*, 949–980.

20. Stronge, W. J. *Impact Mechanics*; Cambridge University Press: Cambridge, MA, 2000.

21. Frey, R.; Gniazdowski, N.; Li, T. H.; Tarzian, F. *Ballistic Shock from Reactive Armor and Explosive Launchers*; U.S. Army Research Laboratory: Aberdeen Proving Ground, MD, to be submitted for publication, 2005.

22. Hertz, H. Über Die Berührung Fester Elastischer Körper (On the Behavior of Solid Elastic Bodies). *J. Reine Angew. Math.* **1882**, *92*, 156–171.

23. Landau, L. D.; Lifshitz, E. M. *Theory of Elasticity*; Pergamon Press: Oxford, 1970; 30–36.

24. Love, A. E. H. *A Treatise on the Mathematical Theory of Elasticity*; Dover: New York, NY, 1955.

25. Leroy, B. Collision Between Two Balls Accompanied by Deformation: A Qualitative Approach to Hertz's Theory. *Am. J. Phys*. **1984**, *53* (4), 346–349.

26. Nesterenko, V. F. *Dynamics of Heterogeneous Materials*; Springer-Verlag: New York, NY, 2001.

27. Allen, M.; Tildesley, D. *Computer Simulation of Liquids*; Oxford: New York, NY, 1987.

28. MatWeb Home Page. http://www.matweb.com (accessed August 2004).

29. Pöschel, T.; Brilliantov, N. V. Extremal Collision Sequences of Particles on a Line: Optimal Transmission of Kinetic Energy. *Phys. Rev. E* **2001**, *63* (021505), 1–9.

30. Jackson, C. M.; Wagner, H. J.; Wasilewski, R. J. *55-Nitinol—The Alloy Tith a Memory: Its Physical Metallurgy, Properties, and Applications*; NASA-SP-5110; National Aeronautics and Space Administration: Washington, DC, 1972.

INTENTIONALLY LEFT BLANK.

Appendix A. Simple Tapered Chain Code [1]

This appendix appears in its original form, without editorial change.

[1] Pfannes, J. Energy Propagation in Granular Chains. M.S. Thesis, State University of New York, Buffalo, NY, May 2003.

```
/* PROGRAM taperchain.cpp

     This program consideres an one dimensional chain of spheres that
     shrink succesively in radius ("tapered chain").  Initially the spheres
     are barely in contact, i.  e.  they just touch each other and are not
     compressed (zero loading).
     The chain ends at both edges at fixed walls.
     The program calculates the interaction of the system once disturbed
     by an instantaneous (delta) impulse exerted on one end of the chain.
     Restitution both between the spheres and between the edge spheres
     and the corresponding wall can be introduced.
     The program does not consider gravity.

     The EOM are solved with the Velocity Verlet algorithm.

     scale of problem: mm-mg-musec (mimimu)
        in this scale unit of force: 1000 N
        in this scale unit of energy: 1 J
                                                                          */

#include <cmath>
#include <iostream>
#include <fstream>
#include <cstdlib>
#include <string>
#include <sstream>

using namespace std;

/************************* ALTERABLE PARAMETER: ***************************/
const int nptles=20;   // total number of particles
const double rho=3.2 /* SiC (mg/mm^3) */, D=0.00326603139013 /* (mm^2/N) */;

const double rlarge = 5.0;       // (radius of large ptle (mm))
const double q = 0.0;            // (tapering factor (%))
const double xn = 2.5;           // (exponent in potential)
const double dt = 0.00001;        // (timestepwidth (musec))
const unsigned int nsteps = 100000000; // (# steps integration loop)
const int idiagp = 20000;         // (stepwidth diagnostics)
const int idump = 20000;          // (stepwidth dump)
const double v1in = 0.0;         // (initial v small ptle (mm/musec))
const double vnin = -0.01;       // initial v large ptle (mm/musec))
const double epsilon = 1.0;     // ((1 - restitution factor) all ptles)
/**************************************************************************/

ofstream readme("taperchain.readme");        // global scope fcts
ofstream EnergyImpulse("taperchain.EneImp");

void radii (double rlocal[]) {
  rlocal[nptles-1] = rlarge;
  if (q == 0)                     // avoid roundoff errors w/out tapering
    for (int i = 0; i < nptles-1; i++)
      rlocal[i] = rlarge;
  else
    for (int i = 2; i < nptles+1; i++)
```

```
      rlocal[nptles-i] = rlocal[nptles-i+1] * (1 - q*0.01);
}

void masses (double r[], double masslocal[]) {
  const double pi = 4 * atan(1.0);
  const double masslarge = (4.0/3.0) * pi * rlarge*rlarge*rlarge * rho;
  masslocal[nptles-1] = masslarge;
  if (q == 0)                       // avoid roundoff errors w/out tapering
    for (int i = 0; i < nptles-1; i++)
      masslocal[i] = masslarge;
  else
    for (int i = 0; i < nptles-1; i++)
      masslocal[i] = r[i]*r[i]*r[i] * masslarge / (rlarge*rlarge*rlarge);
}

void strenghtfac (double r[], double alocal[]) {
  alocal[0] = (2.0 / (5.0 * D)) * (sqrt(r[0]));
  alocal[nptles] = (2.0 / (5.0 * D)) * (sqrt(r[nptles-1]));
  if (q == 0)                       // avoid roundoff errors w/out tapering
    for (int i = 1; i < nptles; i++)
      alocal[i] = (2.0 / (5.0*D)) * (sqrt(0.5*rlarge));
  else
    for (int i = 1; i < nptles; i++)
      alocal[i] = (2.0 / (5.0 * D)) * (sqrt((r[i]*r[i-1])/(r[i]+r[i-1])));
}

// initialpos prints absolute initial positions, not for calculations
void initialpos (double r[], double xInitiallocal[]) {
  if (q == 0)                       // avoid roundoff errors w/out tapering
    for (int i = 0; i < nptles; i++)
      xInitiallocal[i] = (2.0*(i+1) - 1) * rlarge;
  else {
    xInitiallocal[0] = r[0];
    for (int i = 1; i < nptles; i++)
      xInitiallocal[i] = xInitiallocal[i-1] + r[i-1] + r[i];
  }
}

// absolutpos prints absolute positions to ptle files, not for calculations
void absolutpos (double r[], double x[],
             double xInitial[], double xAbsolutlocal[]) {
  for (int i = 0; i < nptles; i++)
    xAbsolutlocal[i] = xInitial[i] + x[i];
}

void computeAccelerations (double x[], double a[], double r[],
                     double acc[], double overbefore[],
                     double mass[], double& pot) {

  pot = 0.0;          // every call calculates new pot contributions

  for (int i = 0; i < nptles; i++)    // zeroing all acc in every call
    acc[i] = 0.0;                     //   (= every timestep)

  /******* potential/force between neighboring ptles *****************/
  for (int i = 0; i < nptles-1; i++) {
    if (x[i] > x[i+1]) {                  // only when overlap
```

```
    double over = x[i] - x[i+1];
    double overnm1 = pow(over, (xn - 1.0));
    pot += over * overnm1 * a[i+1];
    double forceBetw = a[i+1] * xn * overnm1;

    double forceFactor;
    if (overbefore[i+1] < over)         // when compressing
    forceFactor = 1.0;
    else forceFactor = epsilon;         // when decompressing

    forceBetw *= forceFactor;
                                        // dim acc: force
    acc[i] -= forceBetw;                // sign(-): towards smaller x
    acc[i+1] += forceBetw;              // sign(+): towards larger x

    overbefore[i+1] = over;             // update for next timestep
  }
  else overbefore[i+1] = 0.0;           // reset when no overlap
}

/** potential/force between fixed wall (small, x=0) <-> small ptle **/
if (x[0] < 0) {
  double over = - x[0];
  double overnm1 = pow(over, (xn - 1.0));
  pot += over * overnm1 * a[0];
  double forceSmall = a[0] * xn * overnm1;

  double forceFactor;
  if (overbefore[0] < over)
    forceFactor = 1.0;
  else forceFactor = epsilon;

  forceSmall *= forceFactor;

  acc[0] += forceSmall;

  overbefore[0] = over;
}
else overbefore[0] = 0.0;

/*** potential/force between fixed wall (large) <-> large ptle ******/
if (x[nptles-1] > 0) {
  double over = x[nptles-1];
  double overnm1 = pow(over, (xn - 1.0));
  pot += over * overnm1 * a[nptles];
  double forceLarge = a[nptles] * xn * overnm1;

  double forceFactor;
  if (overbefore[nptles] < over)
    forceFactor = 1.0;
  else forceFactor = epsilon;

  forceLarge *= forceFactor;

  acc[nptles-1] -= forceLarge;

  overbefore[nptles] = over;
```

```
  }
  else overbefore[nptles] = 0.0;

  /***** real dim of acc: division by mass **********/
  for (int i = 0; i < nptles; i++)
    acc[i] /= mass[i];
}

void velocityVerletStep (double x[], double v[], double acc[],
                  double a[], double r[], double overbefore[],
                  double mass[], double& pot) {

  for (int j = 0; j < nptles; j++) {
    x[j] += v[j] * dt + 0.5 * acc[j] * dt*dt;
    v[j] += 0.5 * acc[j] * dt;
  }

  computeAccelerations (x, a, r, acc, overbefore, mass, pot);

  for (int j = 0; j < nptles; j++)
    v[j] += 0.5 * acc[j] * dt;
}

void ptleHeader (ofstream* print, int k) {
  (* print) << "# ptle " << k+1 << ": time (musec)" << '\t' << "x (mm)"
          << '\t' << "v (mm/musec)" << '\t' << "a (mm/musec^2)"
          << '\t' << "kin.  E.  (J)" << '\t' << "f (kN)" << '\t'
          << "impulse (mg*mm/musec)" << '\t' << "xRelative (mm)" << '\n';
}

void dumpData (double t, double mass[], double v[], double acc[],
             double r[], double x[],            // scope absolutpos
             double xInitial[], double xAbsolut[],
             ofstream* print, int k) {

  double keDumpPt[nptles];    // new arrays for dumping data
  double vDumpPt[nptles];       // since arrays pass by argument
  double accDumpPt[nptles];       // dump data manipulated
  double xDumpPt[nptles];

  keDumpPt[k] = 0.5 * mass[k] * v[k]*v[k];
  if (keDumpPt[k] < 1.0e-20) keDumpPt[k] = 0.0; // set small values to zero

  vDumpPt[k] = v[k];
  if (vDumpPt[k] < 1.0e-20 && vDumpPt[k] > -1.0e-20) vDumpPt[k] = 0.0;

  accDumpPt[k] = acc[k];
  if (accDumpPt[k] < 1.0e-20 && accDumpPt[k] > -1.0e-20) accDumpPt[k] = 0.0;

  xDumpPt[k] = x[k];
  if (xDumpPt[k] < 1.0e-20 && xDumpPt[k] > -1.0e-20) xDumpPt[k] = 0.0;

  absolutpos (r, x, xInitial, xAbsolut); // calculate absolute pos.

  (* print) << t << '\t' << xAbsolut[k] << '\t' << vDumpPt[k]  << '\t'
          << accDumpPt[k] << '\t' << keDumpPt[k] << '\t'
          << accDumpPt[k]*mass[k] << '\t'
```

```
          << mass[k]*vDumpPt[k] << '\t' << xDumpPt[k] << '\n';
}

void dumpEnergyImpulse (double t, double kelocal, double telocal, double pot,
                  double ptotallocal, double mass[], double v[]) {
  kelocal = 0.0;
  ptotallocal = 0.0;
  double absptotallocal = 0.0;              // scope only within function
  for (int j = 0; j < nptles; j++) {
    kelocal += mass[j] * v[j]*v[j];
    ptotallocal += mass[j] * v[j];
    absptotallocal += mass[j] * abs(v[j]);
  }
  kelocal *= 0.5;
  telocal = kelocal + pot;
  double potDump = pot;

  if (kelocal < 1.0e-20) kelocal = 0.0;    // set very small values to zero
  if (ptotallocal < 1.0e-20 && ptotallocal > -1.0e-20) ptotallocal = 0.0;
  if (telocal < 1.0e-20) telocal = 0.0;
  if (potDump < 1.0e-20) potDump = 0.0;
  if (absptotallocal < 1.0e-20) absptotallocal = 0.0;

  EnergyImpulse.precision(16);
  EnergyImpulse << t << '\t' << kelocal  << '\t' << potDump << '\t'
            << telocal << '\t' << absptotallocal << '\t'
            << ptotallocal << '\n';
}

void readmeInfo (double ke, double pot, double te, double ptotal,
             double ke1in, double kenin, double p1in, double pnin,
             double r[], double xInitial[], double mass[],
             double a[]) {

  readme << '\t' << ":-) *** TAPERCHAIN within walls *** (-:"
       << '\n' << '\n';
  readme << "parameter of this run: " << '\n' << '\n';
  readme << "total number of particles: " << '\t' << '\t' << nptles << '\n';
  readme << "density of particles (mg/mm^3): " << '\t' << rho << '\n';
  readme << "quantity D of particles (mm^2/N): " << '\t' << D << '\n';
  readme << "radius of large ptle (mm): " << '\t' << '\t' << rlarge << '\n';
  readme << "tapering factor (%): " << '\t' << '\t' << '\t' << q << '\n';
  readme << "exponent in potential: " << '\t' << '\t' << '\t' << xn << '\n';
  readme << "timestepwidth (musec): " << '\t' << '\t' << '\t' << dt << '\n';
  readme << "# steps integration loop: " << '\t' << '\t' << nsteps << '\n';
  readme << "stepwidth diagnostics: " << '\t' << '\t'  << '\t' << "every "
       << idiagp << " timesteps" << '\n';
  readme << "stepwidth dump: " << '\t' << '\t'  << '\t' << "every "
       << idump << " timesteps" << '\n';
  readme << "initial v small ptle (mm/musec): " << '\t' << v1in << '\n';
  readme << "initial v large ptle (mm/musec): " << '\t' << vnin << '\n';
  readme << "restitution factor for all ptles: " << '\t' << 1-epsilon << '\n'
       << '\n';
  readme << "total length of run (musec): " << '\t' << dt * nsteps << '\n';
  readme << "total rows recorded for .EneImp file: " << '\t' << '\t'
```

```
      << nsteps/idiagp +1 << '\n';
  readme << "total rows recorded for particle files: " << '\t'
      << nsteps/idump +1 << '\n' << '\n';
  readme << "Initial system info (t=0): " << '\n' << '\n';
  readme << "kin.  E.  (J)" << '\t' << "pot.  E.  (J)" << '\t'
      << "tot.  E.  (J)" << '\t' << "total impulse (mg*mm/musec)" << '\n';
  readme << ke  << '\t' << pot << '\t' << te << '\t' << ptotal
      << '\n' << '\n';
  readme << "kin.  E.  of small particle (J): " << '\t' << '\t' << ke1in
      << '\n';
  readme << "kin.  E.  of large particle (J): " << '\t' << '\t' << kenin
      << '\n';
  readme << "impulse of small particle (mg*mm/musec): " << '\t'
      << p1in << '\n';
  readme << "impulse of large particle (mg*mm/musec): " << '\t'
      << pnin << '\n' << '\n';
  readme << "particle radii (mm): " << '\n';
  for (int i=0; i < nptles; i++) {
    readme << r[i] << '\t';
   }
  readme << '\n' << '\n';
  readme << "initial particle positions (mm): " << '\n';
  for (int i=0; i < nptles; i++) {
    readme << xInitial[i] << '\t';
   }
  readme << '\n' << '\n';
  readme << "total length of one dimensional alignment (mm): " << '\t'
      << xInitial[nptles-1] + r[nptles-1] << '\n' << '\n';
  readme << "particle masses (mg): " << '\n';
  for (int i=0; i < nptles; i++) {
    readme << mass[i] << '\t';
   }
  readme << '\n' << '\n';
  readme << "particle interaction strenghts (0.0316*N/mm^(3/2)): " << '\n';
  for (int i=0; i < nptles+1; i++) {
    readme << a[i] << '\t';
   }
  readme << '\n';
}



int main ( ) {

  double r[nptles], x[nptles], xAbsolut[nptles], xInitial[nptles],
    v[nptles], acc[nptles], mass[nptles], a[nptles+1],
    overbefore[nptles+1], pot;

  /******************** functions *****************************/
  radii (r);
  masses (r, mass);
  strenghtfac (r, a);
  initialpos (r, xInitial);

  /********************** output files ***************************/
  /****** ptle-files *********/
  ofstream print [nptles];
  for (int k = 0; k < nptles; k++) {
```

```
  string filename;
  ostringstream buffer;

  buffer << "taperchain_" << k+1 << ".dat";
  filename = buffer.str();

  print[k].open(filename.c_str()); // convert string to char
}

for (int k = 0; k < nptles; k++)  // header for particles
  ptleHeader(& print[k], k);
/**************************/

// header for .EneImp file
EnergyImpulse << "# time" << '\t' << "kin.  E.  (J)"  << '\t'
          << '\t' << "pot.  E.  (J)" << '\t' << '\t'
          << "total E.  (J)" << '\t' << '\t'
          << "|(total imp.)| (mg*mm/musec)" << '\t'
          << "total imp.  (mg*mm/musec)" << '\n';
/*************************************************************/

for (int i = 0; i < nptles; i++) {     // zeroing
  x[i] = 0.0;          // relative particle positions for calculation
  v[i] = 0.0;
  acc[i] = 0.0;
  overbefore[i] = 0.0;
}
overbefore[nptles] = 0.0;
double t = 0.0;

v[0] = v1in;                          // mind special input data
v[nptles-1] = vnin;

/**************** initial energy info *********************************/
double ke1in = 0.5 * mass[0] * v[0]*v[0];   // initial kE of edge ptles
double kenin = 0.5 * mass[nptles-1] * v[nptles-1]*v[nptles-1];
double p1in = mass[0] * v[0];      // initial impulse of edge particles
double pnin = mass[nptles-1] * v[nptles-1];

computeAccelerations (x, a, r, acc, overbefore, mass, pot);
                                  // call for initial potential energy

double ke = 0.0;                  // checking for initial system energy
double ptotal = 0.0;
for (int i = 0; i < nptles; i++) {
  acc[i] = 0.0;      // reset acc for verlet in case of initial overlap
  ke += mass[i] * v[i]*v[i];
  ptotal += mass[i] * v[i];
}
ke *= 0.5;
double te = pot + ke;                   // initial total system energy

readmeInfo (ke,  pot,  te,  ptotal, ke1in, kenin, p1in, pnin,
          r, xInitial, mass, a);

/****************** begin of timestep loop ********************/
for (unsigned int i = 0; i < nsteps+1; i++) {
```

```
    t = i * dt;

    velocityVerletStep (x, v, acc, a, r, overbefore, mass, pot);

    /*********** check system energy, plot data ******************/
    if ((i % idiagp) == 0) {
      dumpEnergyImpulse(t, ke, te, pot, ptotal, mass, v);
    }

    /********* check particle energy, plot data ******************/
    if ((i % idump) == 0) {
      for (int k = 0; k < nptles; k++) {
      dumpData(t, mass, v, acc,                  // scope dumpData
             r, x, xInitial, xAbsolut,         // scope absolutpos
             & print[k], k);
      }
    }
  }/******************** end of timestep loop *********************/

  readme.close();
  EnergyImpulse.close();

  for (int k = 0; k < nptles; k++)   // closing particle files
    print[k].close();
}
```

INTENTIONALLY LEFT BLANK.

Appendix B. Decorated Tapered Chain Modifications

This appendix appears in its original form, without editorial change.

```
/************************* ALTERABLE PARAMETER: ****************************/
int nptles = 3;               // total number of particles
const double f = 0.9;   // fractional size of interstitial grain w.r.t last
grain
const double rho=4.42;        // TiAlV (mg/mm^3)
const double D = 0.01206;     // TiAlV (mm^2/N)

const double rlarge = 5.0;        // (radius of large ptle (mm))
const double q = 0.0;            // (tapering factor (%))
const double xn = 2.5;            // (exponent in potential)
const double dt = 0.00001;        // (timestepwidth (musec))
const unsigned int nsteps = 100000000; // (# steps integration loop)
const int idiagp = 20000;         // (stepwidth diagnostics)
const int idump = 20000;          // (stepwidth dump)
const double v1in = 0.0;          // (initial v small ptle (mm/musec))
const double vnin = -0.01;        // initial v large ptle (mm/musec))
const double epsilon = 1.0;       // ((1 - restitution factor) all ptles)
/***************************************************************************/

ofstream readme("taperchain.readme");        // global scope fcts
ofstream EnergyImpulse("taperchain.EneImp");

// Generate radii and masses for DTC
void spheres (double rlocal[], double masslocal[]) {
   rlocal[nptles-1] = rlarge; // shifts everything to index starting at zero
   double tapering = 1 - q*0.01;
   const double pi = 4 * atan(1.0);
   const double masslarge = (4.0/3.0) * pi * pow(rlarge,3) * rho;
   masslocal[nptles-1] = masslarge;
   if (q==0 && f==1.0)              // Monodisperse in DTC
        for (int i=0; i<nptles-1; i++) {
            rlocal[i]    = rlarge;
            masslocal[i] = masslarge;
      }
   else if (q==0) {                       // Quasi-Monodisperse: Avoid
roundoff errors without tapering
      for (int i=1; i<nptles-1; i=i+2) {             // Interstitial grains
            rlocal[i] = rlarge*f;
            masslocal[i] = (4.0/3.0) * pi * pow(rlocal[i],3) * rho;
      }
      for (int i=0; i<nptles-1; i=i+2) {             // Non-interstitial
grains
            rlocal[i] = rlarge;
            masslocal[i] = masslarge;
        }
   }
   // non-monodisperse chains
   else {
      for (int i=1; i<nptles-1; i=i+2) {             // Find radii of
interstitial grains
        rlocal[i] = f*pow(tapering,(nptles-1)/2)*rlarge;
        masslocal[i] = (4.0/3.0) * pi * pow(rlocal[i],3) * rho;
      }
        for (int i=nptles-1; i>=0; i=i-2) {                 //Find radii of
non-interstitital grains
        rlocal[i-2] = rlocal[i] * tapering;
            masslocal[i-2] = (4.0/3.0) * pi * pow(rlocal[i-2],3) * rho;
        }
   }
}

void strenghtfac (double r[], double alocal[]) {
  alocal[0] = (2.0 / (5.0 * D)) * (sqrt(r[0]));
  alocal[nptles] = (2.0 / (5.0 * D)) * (sqrt(r[nptles-1]));
```

```
  if (q == 0 && f == 1.0)                 // avoid roundoff errors w/out
tapering
    for (int i = 1; i < nptles; i++)
       alocal[i] = (2.0 / (5.0*D)) * (sqrt(0.5*rlarge));
  else
    for (int i = 1; i < nptles; i++)
      alocal[i] = (2.0 / (5.0 * D)) * (sqrt((r[i]*r[i-1])/(r[i]+r[i-1])));
}

// initialpos prints absolute initial positions, not for calculations
void initialpos (double r[], double xInitiallocal[]) {
  if (q == 0 && f == 1.0 )                    // avoid roundoff errors w/out
tapering
    for (int i = 0; i < nptles; i++)
      xInitiallocal[i] = (2.0*(i+1) - 1) * rlarge;
  else {
    xInitiallocal[0] = r[0];
    for (int i = 1; i < nptles; i++)
      xInitiallocal[i] = xInitiallocal[i-1] + r[i-1] + r[i];
  }
}
```

INTENTIONALLY LEFT BLANK.

Appendix C. Practical Extration and Report Language (PERL) Script for Parametric Studies

This appendix appears in its original form, without editorial change.

```
#!/usr/bin/env perl

# This program automates the considerable task of setting up parametric
studies on the tapered
# spherical elastic 1-D grain problem.  It takes an input file:
taperchain29.cpp and searches
# through it replacing the values of epsilon, q, and N in for loops and
spitting out a file
# in the appropriate directory.  The directories are created on the fly.
# This version uses the updated directories and is looking at initial velocity
on the small
# grain.

$w = 0.1;
$FILE_NAME   = "taperchain28_w01.cpp";
$SOURCE_DIR  = "/home/rldoney";
#$SOURCE_DIR  = "/Users/bob/Work/Classes/Spring 2004/Dr.  Sen study/runs";
$FILE_IN     = "$SOURCE_DIR/$FILE_NAME";
$OUT_DIR     = "/nfs/scratch/rldoney/TiAlV/D.SimpleTapered";
#$OUT_DIR     = "$SOURCE_DIR/TiAlV/D.SimpleTapered/D.Vin_large/";
$EPSILON_CHK = "const double epsilon =";  # Set pattern to match line with
epsilon
$Q_CHK           = "const double q =";               # Set pattern to match
line with q
$N_CHK       = "int nptles=";                  # Set pattern to match line
with N

system("clear");        # clear the screen;

#for($w = 0.0; $w<=0.02; $w+=0.01) {            # Restitution
$epsilon = 1.0 - $w;    # taperchain.cpp program uses epsilon instead of w
directly
print"\n\n::::::::  w=$w \t epsilon = $epsilon  ::::::::\n";
system("date '+DATE: %m/%d/%y%nTIME: %H:%M:%S'");
print"\n";
chdir("$OUT_DIR") or die "Cant open $OUT_DIR";
mkdir("w$w");
chdir("w$w") or die "Cant open $OUT_DIR/w$w";

for($N=3; $N <=20; $N++) {
    mkdir("N$N");
    chdir("N$N") or die "Cant open N$N";

      for($q=0; $q <=10; $q++) {
            mkdir("N$N\q$q");
            chdir("N$N\q$q") or die "Cant open N$N\q$q";
            $CURRENT_DIR = `pwd`;
            chop($CURRENT_DIR);                 # remove trailing \n
            print"Current Dir: $CURRENT_DIR\n";
            $FILE_OUT= "$CURRENT_DIR/$FILE_NAME";
            open(FROM, "$FILE_IN") or die "Cant open $FILE_IN: $!";
            open(TO, ">$FILE_OUT") or die "Cant open $CURRENT_DIR/$FILE_OUT:
$!";
            print"  ";
            system("date '+TIME: %H:%M:%S'");

            while(<FROM>) {   # Read in the file line by line into $_

              # Replacements (Regular expression matching)
              if($w != 0) {
                 s/$EPSILON_CHK \d+\.\d+/$EPSILON_CHK $epsilon/;  # change
epsilon
              }
```

```
              s/$N_CHK\d+/$N_CHK $N/;                          # change N
              s/$Q_CHK \d+\.\d+/$Q_CHK $q\.0/;        # change q

              print TO $_;                # Write the current line with any
changes to TO
              close TO;
             }
             close FROM;

      # Escape to the shell, compile the file, and run it
      # It was unexpected, but we need the ' ' because of the spaces in the
path
      system ("g++ '$FILE_OUT'");
      system ("./a.out");
      chdir("../");
      }
  chdir("../");
  print("\n");
}

system("date '+DATE: %m/%d/%y%nTIME: %H:%M:%S'");
```

INTENTIONALLY LEFT BLANK.

Appendix D. MATLAB Code for Generating Numerical Kinetic Energy Surfaces

This appendix appears in its original form, without editorial change.

```
clc; format compact; format long

% STC directory
cd '/Volumes/Xternal/Individual Study/TiAlV/D.SimpleTapered/D.Vin_large'
pwd
wi   = 0;

qmin = 0;
qmax = 10;
qtot = qmax-qmin + 1;
fileprefix = 'taperchain_';
for w=0.0 : .02 : 0.1
    wi = wi + 1;
    cd (['w',num2str(w)]);
    Ni = 0;
    for N=3:1:20
      Ni = Ni + 1;                    % Since N skips, we need an index for N
      filesuffix = N;                    % For simple tapered chain
      cd (['N',num2str(N)])
      foldername = (['N',num2str(N)]);            % Build name of N# directory
      foldernameq = ([foldername,'q']);           % Build name of N#q
directory
      for q=qmin:qmax
        %qi = q;              % If we ignore the monodisperse case
        qi = q + 1;          % Indices can't be zero, so create qi as an index
        foldername = ([foldernameq,num2str(q)]);    % Foldername is determined
by current q
        cd([foldername])
        file = ([fileprefix,num2str(filesuffix)]);
        filename = ([file,'.dat']);                 % Add the .dat suffix to
current filename
        pwd

        % Largest Grain
        KEinL(Ni,qi,:)   = dlmread([filename],'\t','E2..E12');            %
E(J)       - KE
        %FinL(Ni,qi,:)   = dlmread([filename],'\t','F2..F1202');        %
F(kN)      - Force

        % Smallest Grain
        %t(Ni,qi,:)      = dlmread('taperchain_1.dat','\t','A2..A5002');
             % t(us) - Time
        KEoutS(Ni,qi,:)   = dlmread('taperchain_1.dat','\t','E2..E1502');
      % E(J) - KE
        %FoutS(Ni,qi,:)   = dlmread('taperchain_1.dat','\t','F2..F1202');
      % F(kN) - Force

        % INPUTS
        % =======
        % Maximum input kinetic energy is 1st element (initial velocity)
        % in the largest grain of every chain
        KEmax_in_L(Ni,qi,:)     = KEinL(Ni,qi,1);

        % Maximum input Force is somewhere early on for 1st element.
        %% ANDed portion is to make sure a small peak doesn't occur earlier
        %for i=1:1200
        %    if (FinL(Ni,qi,i+1) < FinL(Ni,qi,i)) && (FinL(Ni,qi,i) > 0.001)
        %        Fmax_in_L(Ni,qi)      = FinL(Ni,qi,i);
        %        break
        %    end
        %end

        % OUTPUTS
        % ========
```

```
        % New technique of normalizing: wrt first peak hitting last grain.
        % peak occurs when comparing the difference between the ith and
        % (i+1)st elements.  when it is less than zero we have just passed a
        % peak
        %% ANDed portion is to make sure a small peak doesn't occur earlier
        for i=1:1200    % Only need a small part of t

            if (KEoutS(Ni,qi,i+1) < KEoutS(Ni,qi,i)) && (KEoutS(Ni,qi,i) >
0.001)
                KEmaxF_out_S(Ni,qi) = KEoutS(Ni,qi,i);
                break
            end

            % For force, since the acceleration is the other way, the sign
            % < goes to >.  And we want only want the magnitude of the force
            %FmaxF_out_S(Ni,qi) = abs(min(FoutS(Ni,qi,:)));
            %if (FoutS(Ni,qi,i+1) > FoutS(Ni,qi,i))
            %    FmaxF_out_S(Ni,qi) = abs(FoutS(Ni,qi,i));
            %    break
            %end
            i = i+1;
        end
        cd ..
        clear foldername
      end
      cd ..
    end
    %Fnorm_in_L    = FmaxF_out_S ./ Fmax_in_L;     % Normalize Fout/Fin per
each specific grain
    KEnorm_in_L    = KEmaxF_out_S ./ KEmax_in_L;     % Normalize Fout/Fin per
each specific grain
    cd '/Volumes/Xternal/Individual Study/TiAlV/D.SimpleTapered/D.Vin_large'

    Ni = linspace(3,20,18);
    qi2 = linspace(qmin,qmax*0.01,qtot);

    % Figure labeling
    if wi == 1
        letter = 'a';
    elseif wi == 2
        letter = 'b';
    elseif wi == 3
        letter = 'c';
    elseif wi == 4
        letter = 'd';
    elseif wi == 5
        letter = 'e';
    else
        letter = 'f';
    end

    % For some reason, these 3-d plots switch the x and y plotting.  The
    % variables are correct, but the ordering was unexpected
    %plot( squeeze( Ft(1,2,:)) , squeeze( Fin(1,2,:) )   )      % N = 3 , q =
1
    subplot(3,2,wi)
      %surf(qi2,Ni,Fnorm_in_L)
      surf(qi2,Ni,KEnorm_in_L)
      xlabel('\bf q')
      ylabel('\bf N_i')
      %if (wi == 1 | wi == 3 | wi == 5)
        zlabel('\bf \it KE_N')
      %end
      text(0,18,0.4,['\it \omega = ',num2str(w)])
```

```
      % subplot labeling based on index of wi
      text(0,18,0.5,['\bf (',letter,')'],'FontSize',14,'FontName','Times')

      axis([0.0 0.1 3 21 0 0.5])
      view(135,10)
      caxis([0 0.5])      % Adjust the limits of the color scheme for Z, must
come before colorbar
      %colorbar
end
cd '/Applications/Physics/Matlab7'
```

Appendix E. Normalization

Normalization has posed some challenges in trying to properly assess the absorption quality of a simple tapered chain (STC). Proper normalization schemes will help the architect better determine which STC is best for which application. Recall that the goal is to measure the energy at the last grain versus the energy put into the system by the first. In general, the functional form will stay the same regardless of the strategy and adjustments in the normalization will simply scale the kinetic energy (KE) surface. In some cases, the output force of each chain is based on the maximum value felt by any possible chain under consideration (i.e., monodisperse and no energy loss).[1] This gives a measure of how one chain is better than another.

In this communication, we have chosen to form the ratio based on the output KE and force felt by each specific chain. This serves to grade the individual effectiveness of any chain without reference to another. In choosing a peak value with this method, one could identify either when the impulse first hits the last grain or look for the absolute maximum peak whenever it may occur. We have chosen to use the former for several reasons. First, it ignores the complexity of nonlinear reverberations which can lead to large peaks at unpredictable times. Second, we argue that this is just as realistic as selecting the maximum value anywhere in the time spectrum.

It turns out that in most cases, the absolute maximum is the first peak. There are special cases where the maximum may occur at later times and this needs to be investigated further. In figure 6 (in the body of the report) for $q = 0.1$, for example, we see the striking occurrence of the secondary pulse about 225 μs being much stronger than the initial arrival at 35 μs. This is one of those instances that disagrees with the way we choose to normalize our KE surfaces. We have investigated this particular case further without including extraneous plots and report the following observations. The effect exists for $N = 15 - 20$ for constant ω. When $N = 20$ is held fixed and restitution is increased, the peak KE once again occurs for the first arrival of the pulse. As q increases, so do the number of collisions and the requisite energy loss (since $\omega \neq 0$). Therefore, it is less likely to find a global peak later in the simulation. The situation is further complicated by the interplay between q and ω.

[1] Pfannes, J. Energy Propagation in Granular Chains. M.S. Thesis, State University of New York, Buffalo, NY, May 2003.

NO. OF
COPIES ORGANIZATION

1 (PDF ONLY) DEFENSE TECHNICAL INFORMATION CTR
DTIC OCA
8725 JOHN J KINGMAN RD
STE 0944
FORT BELVOIR VA 22060-6218

1 US ARMY RSRCH DEV & ENGRG CMD
SYSTEMS OF SYSTEMS INTEGRATION
AMSRD SS T
6000 6TH ST STE 100
FORT BELVOIR VA 22060-5608

1 INST FOR ADVNCD TCHNLGY
THE UNIV OF TEXAS
AT AUSTIN
3925 W BRAKER LN STE 400
AUSTIN TX 78759-5316

1 DIRECTOR
US ARMY RESEARCH LAB
IMNE ALC IMS
2800 POWDER MILL RD
ADELPHI MD 20783-1197

3 DIRECTOR
US ARMY RESEARCH LAB
AMSRD ARL CI OK TL
2800 POWDER MILL RD
ADELPHI MD 20783-1197

3 DIRECTOR
US ARMY RESEARCH LAB
AMSRD ARL CS IS T
2800 POWDER MILL RD
ADELPHI MD 20783-1197

ABERDEEN PROVING GROUND

1 DIR USARL
AMSRD ARL CI OK TP (BLDG 4600)

NO. OF
COPIES ORGANIZATION

5 INST FOR DEFENSE ANALYSES
H BERTRAND
G BOEZER
J HEAGY
I KOHLBERG
M RIGDON
4850 MARK CENTER DR
ALEXANDRIA VA 22311-1882

7 STATE UNIVERSITY OF NEW YORK
DEPT OF PHYSICS
R GONSALVES
B POWELL
S SEN (5 CPS)
239 FRONCZIAK HALL
BUFFALO NY 14260-1500

1 STATE UNIVERSITY OF NEW YORK
DEPT OF MATHEMATICS
B PITMAN
244 MATHEMATICS BLDG
BUFFALO NY 14260-2900

ABERDEEN PROVING GROUND

37 DIR USARL
AMSRD ARL WM
T WRIGHT
AMSRD ARL WM MD
B CHEESEMAN
AMSRD ARL WM T
B BURNS
M ZOLTOSKI
AMSRD ARL WM TA
A BARD
P BARTKOWSKI
R DONEY (10 CPS)
G FILBEY
B FREY
V HERNANDEZ
E HORWATH
T JONES
M KEELE
P KINGMAN
D KLEPONIS
C KRAUTHAUSER
B LEAVY
I LISKO
A MIHALCIN
J RUNYEON
S SCHOENFELD
AMSRD ARL WM TB
R SKAGGS

NO. OF
COPIES ORGANIZATION

AMSRD ARL WM TC
M FERMEN-COKER
AMSRD ARL WM TE
P BERNING
C HUMMER
J POWELL
AMSRD ARL SL BE
B BRUCHEY
T BJERKE

INTENTIONALLY LEFT BLANK.